UARI Research Report No. 30

HYPERSONIC NON-EQUILIBRIUM FLOW AND ITS THERMODYNAMIC RELATIONS

by

Rudolf Hermann

Invited lecture presented at the
4. SPACE SYMPOSIUM
at the University of Goettingen, Germany
October 18-22, 1965

The preparation of this lecture was supported
by the National Aeronautics and Space Administration
under research grant NsG-381

UNIVERSITY OF ALABAMA RESEARCH INSTITUTE
Huntsville, Alabama

November 1965

UARI Research Report No. 30

HYPERSONIC NON-EQUILIBRIUM FLOW AND ITS THERMODYNAMIC RELATIONS

by

Rudolf Hermann

Invited lecture presented at the
4. SPACE SYMPOSIUM
at the University of Goettingen, Germany
October 18-22, 1965

The preparation of this lecture was supported
by the National Aeronautics and Space Administration
under research grant NsG-381

UNIVERSITY OF ALABAMA RESEARCH INSTITUTE
Huntsville, Alabama

November 1965

FOREWORD

The preparation of this lecture was supported by the National Aeronautics and Space Administration under research grant NsG-381.

The visit to the Symposium was sponsored by a cooperation of West-Germany's Aerospace Research Centers.

The author acknowledges the efforts of Mr. Manfred J. Loh, Dipl.-Ing., for valuable assistance in the preparation of this manuscript, and of Mr. Kenneth O. Thompson, Research Associate, for critical comments.

This lecture of research in hypersonic non-equilibrium flow presents the state of the art until September 1965. Co-workers of the author during the past four years in the subject matter being discussed here were, in chronological order, Kenneth O. Thompson, Janardanarao Yalamanchili, Walter Melnik, R. Douglas Archer, and Jurgen Thoenes. Their substantial contributions are gratefully acknowledged.

TABLE OF CONTENTS

LIST OF TABLES AND FIGURES

1. INTRODUCTION

The return of manned and unmanned satellites and space vehicles to the earth's surface with their structure intact is one of the most important problems in astronautics today. During re-entry of a space vehicle through the atmosphere, extremely high velocities are encountered. For instance, at return from a lunar mission nearly parabolic velocity (11.3 km/sec), corresponding to about Mach number 35, is reached. Strong heating, starting behind the shockwave, occurs particularly in the stagnation point region of the re-entering space vehicle (in case of parabolic velocity up to a maximum of 11,000°K at 60 km altitude). Already at much smaller velocities, namely for flight above Mach number 3, air no longer behaves as a perfect gas, and with increasing Mach number, molecular vibration, dissociation, electronic excitation, ionization, and ultimately complete plasma formation progressively take place. These phenomena will change considerably the chemical composition of the air and this change will extend along the body.

Since in most hypersonic applications, the flow has insufficient time to obtain thermodynamic equilibrium, there will generally be non-equilibrium flow in the shock layer. There also exist two limiting cases. Depending on the specific free stream velocity, density, temperature, atmospheric composition, and the absolute size of the body, the flow may be either almost frozen, or the flow may reach very nearly equilibrium.

The calculation of hypersonic flow fields obviously requires thermodynamic and chemical kinetic relations which include the above mentioned real gas effects and the intermediate reactions and products. Since rigorous mathematical expression of such relations would be very complex, this paper uses a simplified air model, formerly introduced and used by the author (Ref. 1,2,3), consisting of oxygen and nitrogen only. For specific flow calculations so far, we further restrict the application to the temperature range in which only oxygen dissociation occurs. Even with these thermodynamic simplifications the computational efforts required to calculate flow around blunt or pointed bodies are very extensive. The use of the simplified air model, however, enables us to show the basic features of equilibrium, non-equilibrium, and frozen flow.

2. NON-EQUILIBRIUM FLOW, HYPERSONIC FLOW FIELDS, AND FLIGHT REGIONS

2.1 Description of Equilibrium Flow, Non-Equilibrium Flow, and Frozen Flow

Before we can discuss non-equilibrium, equilibrium, and frozen flow, we have to define thermodynamic equilibrium of a gas at rest. A gas at rest is, by definition, in thermodynamic equilibrium, if a particular volume of the gas has sufficient, or better infinite, time to bring all its internal modes of energy in equilibrium with the translational energy of the molecular motion. For our consideration those modes are molecular vibration, dissociation, electronic excitation, and ionization. It is justified to assume in our calculations that the rotational energy of the gas molecules is always in equilibrium with the translational energy.

Now considering flow processes of a gas, it is obvious that equilibrium flow is only one limiting case, namely when the changes of the state of the gas flowing along a streamline are so slow that at any point equilibrium is obtained, or stated more exactly, equilibrium is very closely approached. At hypersonic velocities, the time available is, in general, too short for the gas particles which are undergoing rapid density, temperature, and composition changes to reach thermodynamic equilibrium. Hence, in general, we have non-equilibrium flow. The degree of molecular vibration, the degree of dissociation (chemical composition), and the degree of ionization will still change from point to point along the streamline but will not reach thermodynamic equilibrium at any point.

Another limiting case occurs when the gas moves so fast that the internal energy modes have no time to follow the changing density and temperature with the result that the vibrational energy, the energy in dissociation, and the energy in ionization stay very nearly constant. We call this flow frozen; the gas might be vibrationally frozen, and/or chemically frozen (frozen dissociation or no change in degree of dissociation), and/or the gas has frozen ionization.

After this qualitative discussion we can define the thermodynamic behavior more exactly as follows:

At hypersonic velocities, as encountered during re-entry, a major fraction of the free stream kinetic energy is transformed into thermal energy behind the shock wave, causing excited molecular vibration, dissociation, and ionization. These higher energy states of a gas are caused by the collisions of two respective particles, such as molecules, atoms, ions and electrons. Simultaneously, there are also the reverse processes occurring called recombination (of dissociation) or recombination (of ionization), due to another type, the so-called three-body collision. It should be noted that the equilibrium state is a dynamic state where, for otherwise fixed conditions, the processes of dissociation, ionization, and recombination are continuously occurring and are balancing each other. In general, a large number of collisions among the particles is required to equilibrate the energy of molecular vibration, dissociation, ionization, and other modes of excitation with the molecular translational temperature. This means that a finite amount of time is needed even for a gas at rest to approach the state of thermodynamic equilibrium.

The departure from equilibrium of a flowing gas depends upon the ratio of a characteristic translational time needed by the macroscopic motion of the particles to cover a typical distance, relative to the magnitude of the respective relaxation time. The relaxation time is different for each mode of excitation. Hence, hypersonic flow fields are, in general, in some non-equilibrium state. Only under particular circumstances may the flow approach one or the other limit, i.e., equilibrium flow or frozen flow respectively. Theoretically, the frozen state can be defined as a state where the ratio of characteristic translational time to relaxation time approaches zero. Conversely, in case of equilibrium flow, the ratio of characteristic translational time to relaxation time approaches infinity. Considering, for example, dissociation, this means that in frozen flow the chemical composition along a streamline remains constant, independent of the changes of other state variables. In contrast, in equilibrium flow, the composition along a streamline will change if other state parameters change.

Since the characteristic translational time is dependent on the body size, and since relaxation times are dependent on the temperature, density, and to some extent on local composition, it is obvious that non-equilibrium flow fields are generally not similar for geometrically similar bodies even at completely equal free stream conditions; this is a very important fact.

2.2 Hypersonic Flow Fields, Flow Conditions, and Flight Regions During Re-Entry

By far not all phenomena in the complete range of hypersonic high temperature flow problems can be studied and calculated at the present time, because they are too complicated. Therefore, we must concentrate our efforts on the study of those combinations of variables which are today of the greatest engineering concern. This leads us to the study of the hypersonic flow around bodies in the flight corridors, usually plotted in an altitude vs velocity diagram because flight velocities are related to flight altitudes. The relation depends on the aerodynamic configuration, such as a ballistic capsule or a lifting vehicle, on the specific area loading of the vehicle and, of course, on the initial velocity and path angle with which the re-entry begins. Such re-entry flight corridors may also be presented in any state diagram of the gas. The corridors are of great significance because they give in continuous sequence the range of free stream conditions as they will be encountered during re-entry, as well as the range of flow conditions at the important points of the flow field, such as in the stagnation point region. More details can be found in Reference 1 through 3.

Figure 1 is a typical blunt body configuration used for ballistic vehicles. It is a spherically capped cone which,in high speed flight, generates a detached bow shock. The region between the shock wave and the outer edge of the boundary layer, called the inviscid shock layer, has a subsonic region in the vicinity of the stagnation point; farther downstream the flow is supersonic. Both regions of the inviscid shock layer are separated from the body surface by the boundary layer. Altogether then, there are three distinctly different flow regions, which in general must be analyzed with equally different mathematical methods.

For axisymmetric flow at zero angle of attack, flow fields are symmetric with respect to the body axis; and the inviscid portions can be calculated by presently available methods even though they require considerable computational efforts. If the flow with angle of attack is considered and axial symmetry does not exist, analytical methods are not readily available.

The configuration of the Apollo vehicle developed for lunar return is shown in Figure 2, taken from Ref. 4. The capsule is still an axisymmetric blunt body, but typically it descends at some angle of attack (to a maximum of 33°) which is varied for control purposes during re-entry flight. The flow field is completely unsymmetric, thus adding a major complication to the problem. Besides the subsonic-supersonic inviscid shock layer, there is the boundary layer, and behind the body, a viscous separated region. The latter two regions interact in the viscous mixing region which poses almost unsurmountable difficulties for a theoretical analysis. Unfortunately, because of the location of antennas, this is also an important region as far as electromagnetic wave propagation is concerned (see Reference 1).

Before an analysis of the boundary layer or the wake can be made, the inviscid flow field must be known. The initial effort must, therefore, be directed toward the determination of the inviscid flow field. Since air is a rather complicated mixture of gases, especially when dissociation and ionization must be considered, a truly exact representation is not possible at the present time. In order to properly select a model, it is advantageous to first consider the conditions that are encountered along a typical re-entry trajectory in the earth's atmosphere.

In Figure 3, the cross-hatched region in the velocity-altitude diagram indicates the re-entry corridor of manned space capsules from circular orbit around Earth with about 7.9 Km/sec and for lunar return with about 11.3 Km/sec. Also included are equilibrium conditions behind a normal shock; thus the temperature, the pressure, and the density as they occur in the stagnation point region of a blunt body re-entering the earth's atmosphere can be read from the graph. Thermodynamic data for the graph were taken from References 5 and 6.

It is interesting to observe that a major portion of the space vehicle trajectory is approximately parallel to a line p_s = const. The temperature lines at low velocities are practically vertical, that is, the temperature depends only on the square of the velocity. For higher velocities, the temperature depends on both velocity and altitude. The lower density of high altitudes has the effect of increasing the degree of dissociation

which in turn causes a temperature decrease through the transformation of kinetic energy to energy of dissociation. Nevertheless, the stagnation temperature reaches very large values (up to $11,000^{\circ}$ K) in the case of lunar return.

Figure 4, using thermodynamic data from Reference 7, shows in a pressure-enthalpy diagram for air, the temperature T_s and the compressibility factor Z_s behind a normal shock for equilibrium conditions. Also included is the region of re-entering space capsules as before. The square of vehicle velocity u_1^2, is responsible for the main contribution to the total enthalpy. The free stream enthalpy, which depends on the temperature and the density (i.e., on the altitude), is very small and therefore neglected in our presentation.

The compressibility factor behind the normal shock Z_s expresses the number of all particles in a certain volume, which are partially or completely dissociated or ionized, related to the number of particles in the normal state before dissociation and ionization ($Z_s = 1$). Assuming a simplified air model consists of 21% oxygen and 79% nitrogen only, the curve for $Z_s = 1.21$ indicates that nearly all oxygen molecules are dissociated into atoms. $Z_s = 2$ means nearly all oxygen and nitrogen molecules are dissociated. Values of $Z_s > 2$ mean that ionization has taken place. In practice, some ionization will start before dissociation of all nitrogen molecules is accomplished. Also, the formation of NO as well as the existence of other gases will lead to small deviations from this interpretation.

3. THERMODYNAMIC RELATIONS INCLUDING REAL GAS EFFECTS

3.1 The Simplified Air Model

Before we are able to approach flow problems, dissociation of air at rest in equilibrium must be studied. If all the components of the air and all the possible reactions are taken into consideration, the problem becomes very complicated and the system of exact equations can only be solved by large electronic computers.

This task has been undertaken, for example, in Ref. 8 where 6 components of the air, 22 individual reactions, and 28 species have been considered. As a consequence, a system of 56 simultaneous equations had to be solved. Twenty-eight of the equations are linear, the rest are second order or higher.

We prefer to introduce a simplified air model which consists of oxygen and nitrogen only. We will consider only the dissociation of diatomic oxygen and nitrogen to monatomic oxygen and nitrogen. Hence, reactions of oxygen with nitrogen after dissociation are neglected; in particular, that means the formation of nitric oxide, NO, is disregarded. This simplified air model enables us to understand the basic principles with respect to oxygen and nitrogen dissociation, and to obtain equations which can be easily handled and give us the oxygen and nitrogen dissociation with a very good approximation to the so-called exact values of Ref. 8.

The chosen composition of our model air, before dissociation, is 0.21 O_2 and 0.79 N_2, by volume. The oxygen content was very closely approximated, while the remaining gases in atmospheric air, mainly argon and carbon dioxide, were added to the nitrogen fraction. The resulting physical constants as used in the subsequent calculations are summarized in Table 1.

3.2 Dissociation of Oxygen and Nitrogen in Equilibrium

3.2.1 Process of Dissociation and Recombination

With increasing temperature, we have to consider, in addition to the translational and the rotational motions of the particles, the vibrational motion of the atoms of a diatomic molecule. If the raising of the temperature continues, the number and intensity of collisions between the particles increases. In the process of dissociation, e.g.,

an oxygen molecule must collide with some other particle having enough energy to break up the oxygen molecule. The process of dissociation requires a considerable amount of energy, the so-called dissociation energy. For the recombination of two atoms, a triple collision is necessary, the third body carrying away the energy that the two separate atoms must release to form a stable diatomic molecule.

3.2.2 Definition of Degrees of Dissociation α, β

In general, at a given pressure and temperature, only a certain fraction of the molecules are dissociated into atoms. The degree of dissociation can be defined in various ways. We are using the following definition.

Let us denote

n_{O2} = number of oxygen molecules per unit volume in the undissociated mixture

$\bar{n}_{O2}$ = number of oxygen molecules per unit volume in the dissociated mixture

$\bar{n}_{O}$ = number of oxygen atoms per unit volume in dissociated mixture

(n_{N2}, $\bar{n}_{N2}$, $\bar{n}_{N}$ respectively for nitrogen)

Then we define the degree of oxygen dissociation α as the ratio of the number of dissociated oxygen atoms per unit volume to the initial number of undissociated oxygen atoms per unit volume which are, of course, in molecular state, i.e.,

$$\alpha = \frac{\bar{n}_O}{2\,n_{O2}} \tag{3.1}$$

This equation can be interpreted as the ratio of number of moles*, or as the number of particles per unit volume, or as the mass ratio.

We define the degree of nitrogen dissociation β in the same way:

$$\beta = \frac{\bar{n}_N}{2\,n_{N2}} \tag{3.2}$$

The definitions of α and β are chosen such that $\alpha = 1$ or $\beta = 1$ for complete dissociation i.e., when all oxygen or nitrogen molecules, respectively, are split into atoms.

---

*By "moles", we mean the number of particles (of any species) divided by Avogadro's Number.

The fractions of oxygen and nitrogen molecules in our air model before dissociation are expressed and abbreviated as follows:

$$\frac{n_{O2}}{n_{O2}+n_{N2}} = b = 0.21 \tag{3.3}$$

$$\frac{n_{N2}}{n_{O2}+n_{N2}} = (1-b) = 0.79 \tag{3.4}$$

3.2.3 Law of Mass Action

We describe now the individual reaction, first in the generalized symbolic form

$$\nu_1 Q_1 \rightleftarrows \nu_2 Q_2 + \nu_3 Q_3 + \ldots \tag{3.5}$$

Here Q_i stands for molecules or atoms of certain species. ν_i are the stoichiometric coefficients (integers) in this reaction relation. On the left-hand side appears the reactant Q_1 which is stable at low temperatures, and at the right-hand side we find the products Q_2 and Q_3 of the reaction.

The application of thermodynamic principles leads to the so-called "law of mass action" (see Sections 1.15, 1.16 of Ref. 9) and one obtains

$$\frac{p_2^{\nu_2} \, p_3^{\nu_3}}{p_1^{\nu_1}} = K_p(T) \tag{3.6}$$

Here p_i are the partial pressures of the molecules or atoms of the species Q_i. K_p is a function of temperature only and is called the pressure equilibrium constant of this particular reaction. If this reaction is a dissociation, K_p is related to the energy of dissociation, as seen in Eq. (3.10).

In order to be more specific, let us consider the example of the oxygen dissociation:

$$O_2 \rightleftarrows 2O \tag{3.7}$$

For this reaction, we have $\nu_1 = 1$, $\nu_2 = 2$, and $\nu_3 = 0$. The energy of dissociation D^+ is defined by (Ref. 9):

$$D^+ = \left(\frac{\partial q}{\partial \alpha}\right)_{p,T} \tag{3.8}$$

where q is the heat addition and α the degree of dissociation. It follows from this law that the right-hand side of Eq. (3.8) is $\partial h/\partial \alpha$. Thus we obtain

$$D^+ = h_1 - h_2 \tag{3.9}$$

D^+ is the energy necessary to dissociate completely a unit mass of one species in the molecular state, at constant pressure and temperature. Here h_1 is the enthalpy of the gas in the atomic state and h_2 the enthalpy in the molecular state.

3.2.4 The Pressure Equilibrium Constants $K_{p\alpha}$ and $K_{p\beta}$

The following differential equation for the pressure equilibrium constant K_p can be obtained

$$\frac{d \ln K_p}{dT} = \frac{D^+}{R_2 T^2} \tag{3.10}$$

R_2 is the gas constant per unit mass of the molecular species. The dissociation energy D^+ is, in general, a function of T. However, often this variation is rather small, for instance, in the case of oxygen dissociation between 3000 °K and 5000 °K. If D^+ is assumed constant, Equation (3.10) can be integrated and furnishes

$$K_p = \text{const.}\ e^{-\frac{D^+}{R_2 T}} \tag{3.11}$$

The constant for oxygen, calculated from data given in Ref. 10, is 6.16×10^6 atm. In Eq. (3.11) the following combination of parameters occurs

$$\frac{D^+}{R_2} = D' \tag{3.12}$$

which has the dimension of a temperature and is called the characteristic temperature for dissociation. Its values are

$$D' = 59{,}000\ ^\circ K \text{ for oxygen}$$
$$D' = 113{,}000\ ^\circ K \text{ for nitrogen.}$$

Equilibrium constants for oxygen $K_{p\alpha}$ and for nitrogen $K_{p\beta}$ are shown in Figure 5 as functions of temperature in the range from 2,000 to 10,000°K. These are based on values given in Ref. 11 up to 6,000°K; above this temperature they are taken from Ref. 12.

3.2.5 Degree of Oxygen and Nitrogen Dissociation as Function of Pressure and Temperature

We start with the reaction equation for our simplified air model, but include dissociation of both oxygen and nitrogen.

$$n_{O2}O_2 + n_{N2}N_2 \rightleftarrows \bar{n}_{O2}O_2 + \bar{n}_{N2}N_2 + \bar{n}_O O + \bar{n}_N N \tag{3.13}$$

As mentioned before, n_i and $\bar{n}_i$ are the number of moles of the particular species, which are also proportional to the number of particles in a certain volume. We will write the conservation of mass for oxygen and nitrogen and observe that one mole of diatomic oxygen or nitrogen gives two moles of mon-atomic oxygen or nitrogen.

$$2n_{O2} = 2\bar{n}_{O2} + \bar{n}_O \tag{3.14}$$

$$2n_{N2} = 2\bar{n}_{N2} + \bar{n}_N \tag{3.15}$$

Now we consider the individual reactions and obtain, according to the law of mass action Eq. (3.6), the following equations with the equilibrium constants $K_{p\alpha}$ and $K_{p\beta}$

$$K_{p\alpha} = \frac{p_O^2}{p_{O2}} = \frac{\bar{n}_O^2}{\bar{n}_{O2}} \frac{p}{\Sigma\bar{n}} \tag{3.16}$$

$$K_{p\beta} = \frac{p_N^2}{p_{N2}} = \frac{\bar{n}_N^2}{\bar{n}_{N2}} \frac{p}{\Sigma \bar{n}} \tag{3.17}$$

Here p_i is the partial pressure of the component in the dissociated mixture, while p is the total pressure of the mixture, measured in atmospheres. $\Sigma \bar{n}$ is the total number of moles in the dissociated state, the right hand side of Eq. (3.13). This is a consequence of the fact that the sum of the partial pressures must be equal to the total pressure.

This system of four equations (3.14), (3.15), (3.16), and (3.17) contains four unknowns ($\bar{n}_{O2}$, $\bar{n}_{N2}$, $\bar{n}_O$, $\bar{n}_N$) if pressure p, temperature T (and therefore K_p), and the original molar composition n_{O2}, n_{N2} are given. It can be reduced to two coupled quadratic equations for α and β which must be solved simultaneously by trial and error. An explicit solution with two separate quadratic equations for α and β are obtained if we make use of the physical fact as mentioned before, that oxygen is almost completely dissociated before dissociation of nitrogen begins. Then we have for that temperature range where only oxygen dissociation occurs $\bar{n}_N = 0$ and $\bar{n}_{N2} = n_{N2}$, and therefore

$$\Sigma \bar{n} = \bar{n}_{O2} + \bar{n}_O + n_{N2} \tag{3.18}$$

Equation (3.16) can be transformed with the aid of the equations (3.1), (3.3), (3.14), and (3.18). Thus we obtain

$$\frac{K_{p\alpha}}{p} = \frac{4\,b\,\alpha^2}{(1-\alpha)(1+b\alpha)} = \frac{4\alpha^2}{4.762 - 3.762\alpha - \alpha^2} \tag{3.19}$$

If temperature and pressure are given, the left-hand side is known with the aid of Fig. 5, and α can be calculated. This formula is valid for $0 < \alpha < 1$.

For higher temperatures, both oxygen and nitrogen will dissociate. However, the solution will be simplified again due to the same physical facts mentioned above. With increasing temperature (at fixed pressure), we reach the point, where oxygen is almost completely dissociated, when nitrogen starts to dissociate $\bar{n}_{O2} = 0$ and $\bar{n}_O = 2\bar{n}_{O2}$.

Under this assumption, and with eq. (3.14), we obtain for the temperature range, where nitrogen dissociation is present:

$$\Sigma \bar{n} = 2n_{O2} + \bar{n}_{N2} + \bar{n}_{N} \tag{3.20}$$

In order to evaluate eq. (3.17) for $K_{p\beta}$, we introduce eq. (3.20) and the definition of the degree of nitrogen dissociation (3.2). We are eliminating n_{N2} by eq. (3.15) and we are introducing the numerical value for the ratio n_{N2}/n_{O2} from eqs. (3.3) and (3.4). This finally results in the equation for nitrogen dissociation

$$\frac{K_{p\beta}}{p} = \frac{4\beta^2}{\frac{2b}{(1-b)}(1-\beta) + (1-\beta^2)} = \frac{4\beta^2}{1.5316 - 0.5316\beta - \beta^2} \tag{3.21}$$

The degree of oxygen dissociation α and nitrogen dissociation β are calculated for the simplified air model using eqs.(3.19) and (3.21) as function of temperature and pressure and presented in Fig. 6. It can be seen that the dissociation for both species increases for a certain pressure with increasing temperature, and for a certain temperature with decreasing pressure. Note that at 5000 °K and at the pressure of 1 atmosphere, the oxygen dissociation is almost complete(α close to 1.0) while the nitrogen dissociation for the same pressure just starts(β approximately 0.01). This illustrates the fact that oxygen and nitrogen dissociation are practically uncoupled. This is a result of the markedly different values $K_{p\alpha}$ and $K_{p\beta}$ at a given temperature. Fig. 5 shows that between 4000° and 6000° K, $K_{p\alpha}$ is a factor of 10^6 to 10^4 larger than $K_{p\beta}$.

3.3 Thermal Equation of State for Oxygen Dissociation Only

3.3.1 Simplified Air Model with Restriction to Oxygen Dissociation

The task of the calculation of hypersonic flow through nozzles or around blunt and pointed bodies, as presented in Sections 4, 5, and 6, is so substantial that we will further simplify our air model. We will introduce an additional restriction, namely to oxygen dissociation only. In other words, the range of application expressed in the appropriate ranges of temperature and pressure is such that only oxygen may dissociate. Even with these simplifications and restrictions, the resulting thermodynamic equations are still complex. This air model permits us to gain insight into the distinct features

of non-equilibrium flow phenomena with a minimum of computational effort, which, as it will be seen, is still large.

3.3.2 Derivation of Thermal Equation of State

We will denote the number of particles of the ith species per unit volume of the undissociated mixture with n_i and that of the dissociated mixture with $\bar{n}_i$, and the mass of one particle of the ith species with m_i.

The density of the mixture becomes

$$\rho = \sum_i m_i \bar{n}_i \tag{3.22}$$

Assuming that the individual species obey the perfect gas law, a very important assumption, the total pressure of the mixture is the sum of its partial pressures, or

$$p = \sum_i p_i = \sum_i \rho_i R_i T \tag{3.23}$$

The specific gas constant of each species is given by

$$R_i = \frac{kN_A}{M_i} = \frac{k}{m_i} \tag{3.24a}$$

Combining the three last equations, we obtain the pressure, and dividing it by equation (3.22), we obtain the equation of state as

$$\frac{p}{\rho} = kT \frac{\sum_i \bar{n}_i}{\sum_i m_i \bar{n}_i} \tag{3.24b}$$

We have in the mixture at any state, $\bar{n}_O$ particles of atomic oxygen, $(1-\alpha)n_{O2}$ particles of molecular oxygen and n_{N2} particles of molecular nitrogen. We must also observe that the mass $m_{O2} = 2m_O$ and $m_{N2} = 2m_N$. Inserting those values in eq. (3.24b) and also using eq. (3.1) and equation (3.3), one obtains:

$$\frac{p}{\rho} = (1 + b\alpha)RT = ZRT \tag{3.25}$$

where

$$Z = (1 + b\alpha) \tag{3.26}$$

and numerically

$$b = 0.21 \tag{3.3}$$

Here R is the gas constant of the undissociated gas. Z is called the compressibility factor (see Section 2.2 and Fig. 4). A more detailed derivation of the thermodynamic equations of this and the following thermodynamic sections can be found in Ref. 13.

3.4 Equations for Internal Energy and Enthalpy for Oxygen Dissociation Only

3.4.1 Energy States of a Gas Particle; and Partition Functions

The thermodynamic properties of a gas may be derived from its partition function. Details concerning the partition function may be found in texts on statistical thermodynamics (Ref. 14, 15, 16). We will only summarize those relations that are needed for our calculations. The partition function is closely related to the energy of the particle. In our case, the energy may be due to the translational, rotational, or vibrational motion of the particle, and at higher temperatures due to the motion of the electrons within the particle. Assuming that no coupling exists between the different modes of excitation, the partition function may be written as the product

$$Q = Q_t Q_r Q_v Q_e \tag{3.27}$$

The factors on the right hand side are the partition functions associated with the translational, rotational, vibrational, and electronic energy levels of the particle. For diatomic molecules these factors are:

$$Q_t = \left(\frac{2\pi mkT}{h^2}\right)^{\frac{3}{2}} \frac{kT}{p} \tag{3.28}$$

$$Q_r \simeq \frac{8\pi^2 I kT}{\varkappa h^2} = \frac{T}{\varkappa \theta_r} \tag{3.29}$$

$$Q_v = (1 - e^{-\frac{\theta}{T}})^{-1} \tag{3.30}$$

$$Q_e = \sum_{i=0}^{n} g_i e^{-\frac{\epsilon_i}{kT}} \tag{3.31}$$

For monatomic particles, such as oxygen or nitrogen atoms, which have no mode of rotational or vibrational excitation, the respective partition functions take the value unity. The contribution of those modes to the internal energy then becomes zero. Table 2 presents atomic and molecular constants which were used in our calculations. Note that in eq. (3.31), ϵ_i is the energy of the ith state of a gas particle, and g_i is the degeneracy, that is the number of states of a particle which has this same energy level.

In the following section we shall need Q_c and Q_p, the partition functions for the standard state of unit concentration and of unit pressure, respectively. They are functions of temperature only, and in terms of the total partition function, they are given by

$$Q_c = \frac{p}{kT} Q \tag{3.32}$$

$$Q_p = p\, Q \tag{3.33}$$

3.4.2 Internal Energy Equation

According to statistical thermodynamics, the internal energy per kilomole of a pure gas is given by

$$e = R^* T^2 \frac{d \ln Q_c}{dT} \tag{3.34}$$

Since the total partition function is a product of the individual partition functions and equation (3.34) has a logarithmic character, one sees that the contribution of the various energy modes to the internal energy are additive. We insert in eq. (3.34) the partition function (3.32) and (3.27) with its components (3.28) through (3.30). At the same time, in the range of temperature which we have under consideration, we can neglect the electronic excitation (3.31). (We also observe that atomic oxygen consists of monatomic particles, while oxygen molecules and nitrogen molecules are diatomic particles.) As a result, we obtain

$$e_O = \frac{3}{2} R^* T \tag{3.35}$$

$$e_{O2} = \frac{5}{2} R^* T + \frac{\theta_{O2} R^*}{e^{\theta_{O2}/T} - 1} \tag{3.36}$$

$$e_{N2} = \frac{5}{2} R^* T + \frac{\theta_{N2} R^*}{e^{\theta_{N2}/T} - 1} \tag{3.37}$$

It is obvious that in the above expressions it is assumed that the vibrational temperature and rotational temperature are always in equilibrium with the translational temperature.

The internal energy of the gas mixture, E, is the weighted sum of the internal energies of each species due to the various modes of excitation (translation, rotation, vibration) and of the dissociation energy of the dissociating component,

$$E = \sum_i f_i e_i + \frac{f_O}{2} D_{O2} \tag{3.38}$$

This is called the internal energy equation for the mixture. f_i denotes the mole fractions for the dissociated mixture which are obtained as

$$f_O = 2b \frac{\alpha}{Z} \tag{3.39}$$

$$f_{O2} = b \frac{1 - \alpha}{Z} \tag{3.40}$$

$$f_{N2} = (1 - b) \frac{1}{Z} \tag{3.41}$$

Equation (3.39) has the factor 2 because each oxygen molecule which dissociates will produce two atoms of oxygen. If we have one mole of gas before dissociation, then we will have Z moles after dissociation. Hence, the factor Z occurs in the denominator of all mole fractions, in order to refer the number of particles to one mole. We do not present here the complete equation for the internal energy in detail because it is much more practical to use the equation for the enthalpy given in the next section.

3.4.3 Enthalpy Equation

The enthalpy of the gas mixture is defined in the same way as is the enthalpy of a gas with only one component.

$$h = E + \frac{p}{\rho} \tag{3.42a}$$

E is calculated according to eq. (3.38) with the mole fractions according to (3.39), (3.40), (3.41) and the energy of the particles of the components according to (3.35), (3.36), and (3.37). We have to observe that

$$M_\alpha = \frac{M}{Z} \tag{3.42b}$$

which relates the molecular weight of the dissociated mixture M_α to that of the undissociated air M. The second term in eq. (3.42) is substituted from eq. (3.25). Note that we switch from the universal gas constant R^*, with units (J/kmol ^oK) to the gas constant of the undissociated gas, R, with unit (J/kg ^oK). The enthalpy equation (per kilogram) is finally obtained as

$$h = R\left[b\alpha D'_{O2} + \frac{3}{2} b\alpha T + \frac{7}{2} T + (1-\alpha)\, b \left(\frac{\theta_{O2}}{e^{\theta_{O2}/T} - 1} \right) + (1-b) \frac{\theta_{N2}}{e^{\theta_{N2}/T} - 1} \right] \tag{3.43}$$

θ is the characteristic temperature of vibration, and D' the characteristic temperature of dissociation. This enthalpy is then given in joules per kilogram.

3.5 Dissociation and Recombination Rate Equations for Oxygen Dissociation

3.5.1 Departure from Equilibrium

In general, a large number of collisions among the particles is required to bring the molecular vibrations, dissociation, and higher degrees of excitation in equilibrium with the local translational temperature. This means that a finite amount of time is needed for the gas properties to approach thermodynamic equilibrium. The departure from equilibrium of a flowing gas is characterized by the magnitude of this relaxation time relative to some translational time needed by the particles to move over a characteristic distance on a body or within a nozzle. Since only oxygen dissociation is considered, only one chemical rate equation is needed. Vibrational relaxation should be also

included when higher accuracy is required. In view of the complexity that would be introduced if the coupling between vibration and dissociation were treated, it is felt that it is justified to assume the vibrations to be in equilibrium.

3.5.2 Dissociation and Recombination Rate Equation

The number of oxygen atoms, in either molecular or atomic form, per unit mass of the gas can be written as

$$C = 2b \frac{N_A}{M} \tag{3.44}$$

The number of free oxygen atoms per unit volume of the gas is then

$$\bar{n}_O = C \alpha \rho \tag{3.45}$$

We are now interested in the number of oxygen atoms generated per unit volume and unit time, denoted by w. From eq. (3.45) together with the over all continuity equation, one can obtain the following relation between the net production of oxygen atoms generated and the gradient of the degree of oxygen dissociation, α as

$$w = C \rho (\vec{q} \cdot \text{grad } \alpha) \tag{3.46}$$

The net rate of oxygen atoms generated by unit volume of the gas is

$$w = \left(\frac{d\bar{n}_O}{dt}\right)_{diss} + \left(\frac{d\bar{n}_O}{dt}\right)_{rec} \tag{3.47}$$

The first term is positive because dissociation increases the number ot tree atoms; the second term is negative because recombination decreases the number of free oxygen atoms. The process of dissociation or recombination which may occur in our present air model can be described by

$$O_2 + M_i \underset{k_{r,i}}{\overset{k_{d,i}}{\rightleftharpoons}} O + O + M_i \tag{3.48}$$

In the process of dissociation, the oxygen molecule must collide with another particle M_i of the ith species, either an oxygen atom or molecule or a nitrogen molecule in our air model. k_d is the dissociation rate constant which depends strongly on the type

of the colliding body M_i. The recombination process is the inverse of the dissociation. In order to occur, it is necessary that two oxygen atoms collide at the same time with a third body M_i, which is able to carry away the energy in such a way that two atoms can form a stable diatomic oxygen molecule. It is obvious that also the recombination rate constant will depend on the type of the colliding body M_i. Obviously, recombination requires a three-body collision and hence it is much more rare than the collision which produces dissociation. The number of particles per unit volume that may act as colliding bodies will be for our air model

$$\bar{n}_M = \bar{n}_O + \bar{n}_{O2} + \bar{n}_{N2} \tag{3.49}$$

Adding the species together, we obtain after some calculation

$$\bar{n}_M = \frac{C\rho Z}{2b} \tag{3.50}$$

From the law of mass action, discussed in Section 3.2.3, it follows that the rate of change of concentration is proportional to the product of the concentrations, raised to the power of the stoichiometric coefficients. The application to our specific process of dissociation expressed in eq. (3.48) gives the rate of production of oxygen atoms

$$\left(\frac{d\bar{n}_O}{dt}\right)_{diss} = k_d \bar{n}_{O2} \bar{n}_M \tag{3.51}$$

The rate of the disappearance of oxygen atoms due to recombination is given in a similar way by

$$\left(\frac{d\bar{n}_O}{dt}\right)_{rec} = -k_r \bar{n}_O^2 \bar{n}_M \tag{3.52}$$

Note that the dissociation rate depends on the first power while the recombination rate depends on the third power of the free oxygen atoms, a consequence of the two and three body collisions. k_d and k_r are the temperature dependent reaction rate "constants" for dissociation and recombination respectively. They will be discussed in more detail in Section 3.5.4.

3.5.3 Net Production and Source Function

In order to obtain the net rate of oxygen atoms generated, we substitute (3.51) and (3.52) into (3.47) and obtain

$$w = k_d \bar{n}_{O2} \bar{n}_M - k_r \bar{n}_O^2 \bar{n}_M \tag{3.53}$$

For local thermodynamic equilibrium, the net rate of oxygen atoms generated vanishes, i.e., $w = 0$. Hence,

$$\frac{k_d}{k_r} = \frac{\bar{n}_O^2}{\bar{n}_{O2}} = K_c \tag{3.54}$$

where K_c is the concentration equilibrium constant for the considered reaction. Now we make the important assumption that the above relation, derived for equilibrium, is also valid when the flow is not in chemical equilibrium. Then we substitute equations (3.45) and (3.49) into equation (3.53) and also use equation (3.54) to eliminate k_r, because the recombination rate constant is generally not too well known, while k_d and K_c are much better known. This furnishes

$$w = \frac{C^3 \rho^3 Z k_d}{2b} \left[\frac{(1-\alpha)}{2C\rho} - \frac{\alpha^2}{K_c} \right] \tag{3.55}$$

Substituting this oxygen atom generation rate into equation (3.46), the desired rate equation finally is

$$\vec{q} \cdot \text{grad } \alpha = F \tag{3.56}$$

where

$$F = \frac{C^2 \rho^2 Z k_d}{2b} \left[\frac{(1-\alpha)}{2C\rho} - \frac{\alpha^2}{K_c} \right] \tag{3.57}$$

It is important to see that the dissociation process is proportional to the density and the available oxygen molecules, while the recombination process is proportional to the square of the density and the square of the number of oxygen atoms already dissociated.

3.5.4 Reaction Rate Constants

The processes of dissociation and recombination occur at finite rates. The rate "constants" for both processes were defined in equations (3.51) and (3.52). In order to evaluate the rate equation (3.57) we still need an expression for the dissociation rate constant. Ordinary kinetic theory is not completely adequate to predict these rate constants. In practice, the rate constants are usually given in a form similar to the one which was first suggested by Arrhenius and based largely on experimental data, namely,

$$k_d = S\, e^{-E_d/R^*T} \qquad (3.57\ a)$$

where for dissociation, E_d is the activation energy for dissociation and S the corresponding frequency factor.

A comprehensive review of recent work carried out in the field was given by Wray (Ref. 17). His values will be used in the present investigation.* Due to the simplification introduced, eq. (3.51) and (3.52) were written with a single rate constant each for dissociation and recombination. In order to account for the influence of the catalytic species, we will use a dissociation rate constant, which is averaged with respect to population, of the form

$$k_d = \sum_i f_i k_{d,i} \qquad (3.58)$$

where the f_i are the mole fractions and where the $k_{d,i}$ denote the dissociation rate constants (for oxygen) with the ith species acting as catalyst.

Using now the mole fractions as given in eq. (3.39) and (3.41) and Wray's values, the oxygen dissociation rate constant is

$$k_d = \frac{2.5 \cdot 10^8}{T N_A} \left(\frac{D}{R^*}\right)^{1.5} e^{-\frac{D}{R^*T}} \left(\frac{41\,b\alpha + 7b + 2}{1 + b\alpha}\right) \qquad (3.59)$$

with the dimension (m^3/particle sec). It is seen that the dissociation rate "constant" is actually a function of temperature T, and composition α. Fig. 7 shows the range of this equation for α between 0 and 1, together with the values of other authors for various colliding bodies.

---

*See footnote on page 24

3.6 Equilibrium Constants for Oxygen Dissociation Calculated From Statistical Thermodynamics

3.6.1 Concentration Equilibrium Constant K_c

In order to evaluate the rate equation and to calculate the equilibrium composition for our air model, the equilibrium constant as function of the temperature is needed. The concentration equilibrium constant has been expressed previously according to eq. (3.54).

$$K_c = \frac{k_d}{k_r} = \frac{\bar{n}_O^2}{\bar{n}_{O2}} \tag{3.54}$$

3.6.2 Pressure Equilibrium Constant K_p

The pressure equilibrium constant K_p is defined in terms of the partial pressure as derived before (see eq. (3.16) and (3.17)). It depends on the partition functions and the energy of the products and the reactants. For the oxygen dissociation reaction the equilibrium constant becomes

$$K_p = \frac{Q_p^2(O)}{Q_p(O_2)} \; e^{-\frac{D'}{T}} \tag{3.60}$$

Because the equilibrium constant contains the ratio of the partition functions, we cannot neglect the electronic contribution as we did in calculating the internal energy. However, only those energy levels which give an appreciable contribution within the temperature range in which our air model is valid were considered. Equations (3.27) through (3.31), and (3.33) are substituted into (3.60). Using the numerical values one obtains

$$K_p = A_p T^{3/2} \left[1 - e^{-\frac{2270}{T}}\right] \frac{\left[5 + 3e^{-228/T} + e^{-326/T}\right]^2}{3 + 2e^{-11390/T}} \left[e^{-\frac{59366}{T}}\right] \tag{3.61}$$

where $A_p = 2.444056 \cdot 10^5$ for K_p N/m^2

$= 2.412096$ for K_p atm

Explicit expressions for the constant A_p are given both in Newton's per square meter, as well as in atmospheres. The concentration equilibrium constant, described before, is related to the pressure equilibrium constant by

$$K_c = \frac{K_p}{kT} \tag{3.62}$$

and has the dimension (particles/m^3) if K_p is used in (N/m^2).

3.6.3 Equilibrium Flow Relation

For equilibrium flow a relation between the equilibrium constant and the degree of dissociation is very useful and necessary in order to carry out such calculations. This can be obtained by considering the fact that for local equilibrium, the net rate of production of oxygen atoms w must vanish. If we set eq. (3.55) to zero we obtain

$$\frac{K_c (1-\alpha)}{2C\rho} - \alpha^2 = 0 \tag{3.63}$$

Using eq. (3.25) to substitute ρ and (3.44) to substitute C, and using eq. (3.62) to change from the concentration to the pressure equilibrium constant, one obtains

$$\frac{K_p(T)}{p} = \frac{4\alpha^2}{(b^{-1} + \alpha)(1-\alpha)} \tag{3.64}$$

The above equation is identical with equation (3.19) obtained earlier by different means. The equation relates the composition for any state of thermodynamic equilibrium within the range of oxygen dissociation to the pressure and the pressure equilibrium constant, which is a function of temperature only according to (3.61). It has to be used for any flow calculations which assume equilibrium conditions.

Footnote from page 22:
In Reference 17 and others, as well as in this paper, the activation energy for dissociation, E_d, is assumed equal to the energy of dissociation D. This follows from the observation that the activation energy for recombination of 2 atoms is nearly zero (Ref. 40).

4. NON-EQUILIBRIUM FLOW WITH OXYGEN DISSOCIATION THROUGH A HYPERSONIC NOZZLE

4.1 Assumptions and Basic Equations

The flow through a hypersonic Laval nozzle of small or moderate cone angle is almost one-dimensional. Hence, it is much easier to understand than the hypersonic flow around bodies, and is also much easier to treat mathematically, because the flow is described by ordinary instead of partial differential equations. Hence, flow through a nozzle is well suited to demonstrate equilibrium, non-equilibrium, and frozen flow. In fact, for the practical cases calculated below, all three regimes occur in the same nozzle in sequence due to the expansion from high to low temperatures and densities.

We will first consider the flow through a hypersonic nozzle up to a Mach number of about 15 for various supply conditions, nozzle geometries, and sizes. The flow through a hypersonic nozzle has been calculated under the assumption of one-dimensional flow with the basic thermodynamic relations specified in Section 3 for the real gas effects and particularly for the simplified air model. In addition, viscosity, diffusion, and heat conductivity of the air are neglected. Five equations have been established. The continuity equation and the momentum equation in the x direction are of the conventional form and, hence, are omitted here. In addition, there are: the equations of energy containing the enthalpy, the equation of state, and the rate equation, all of which are derived in Section 3 (Eqs. 3.38, 3.25, 3.59). The 5 unknowns are velocity u, pressure p, temperature $\bar{T}$, density ρ, and degree of dissociation α. In addition, the energy equation (3.38) contains the enthalpy h, which is expressed by $\bar{T}$ and α through equation (3.43). It was possible to eliminate pressure p and velocity u from the 5 equations and, hence, 3 ordinary differential equations remain to be solved (Eqs. 4.1, 4.2, 4.4).

$$\frac{d\alpha}{dx} = \frac{C^2 \rho^2 (1+b\alpha)\, k_r \left[\frac{K_c}{2C} (1-\alpha) - \rho \alpha^2 \right]}{2b \frac{\dot{m}}{A^*} \frac{A^*}{A}} \tag{4.1}$$

$$\frac{d\rho}{dx} = \frac{RZT\left(\frac{A}{A^*}\right)^2 \rho^3 \left[\frac{b}{\bar{Z}}\frac{d\alpha}{dx} + \frac{1}{\bar{T}}\frac{dT}{dx} - \frac{A^*}{A}\frac{d}{dx}\left(\frac{A}{A^*}\right)\right]}{(\dot{m}/A^*)^2(1-K)} - \rho\frac{A^*}{A}\frac{d}{dx}\left(\frac{A}{A^*}\right), \tag{4.2}$$

$$K \equiv \frac{RZT\,\rho^2\left(\frac{A}{A^*}\right)^2}{\left[\frac{\dot{m}}{A^*}\right]^2}\;; \qquad b \equiv \frac{n_{O2}}{n_{O2}+n_{N2}} \tag{4.3}$$

$$\frac{dT}{dx} = \frac{(1-K)\left[\frac{\partial h}{\partial \alpha} - \frac{RTb}{1-K}\right]\frac{d\alpha}{dx} + RZT\frac{A^*}{A}\frac{d}{dx}\left(\frac{A}{A^*}\right)}{RZ - \frac{\partial h}{\partial T}(1-K)} \tag{4.4}$$

This system shows the derivatives for α, ρ, and T with respect to x. It is noted that the derivative of α depends only on the state of the gas and the area. The derivative of the density contains, besides the state of gas, the derivatives of α, T, and the area change. The derivative of the temperature contains also the derivatives of α and the area change but, in particular, two partial derivatives of the enthalpy with respect to α and T.

4.2 Flow Calculations

It can be proven exactly with the methods of irreversible thermodynamics, that equilibrium flow with changing degree of dissociation, if adiabatic, is also reversible and isentropic. The same is valid for adiabatic frozen flow with constant chemical composition. However, the general case of adiabatic non-equilibrium flow is not isentropic.

Calculations have been carried out for the flow assumed to be in equilibrium as well as for the general case of non-equilibrium flow, in order to compare the results of the two concepts. In the subsonic portion of the nozzle, because of the low velocity, the flow is assumed to be in equilibrium up to the throat, but this assumption should be checked for any particular case. The subsonic expansion is then isentropic; consequently, the temperature, compressibility factor, and the enthalpy can be determined from a Mollier chart for arbitrary values of the pressure, following a line of const. entropy. The corresponding density and velocity can then be calculated. The throat

conditions can be found by calculating the mass flux as function of x which must be a maximum at the throat.

In the supersonic portion of the nozzle and for the equilibrium flow calculation, the same procedure has been followed. Such results have been presented by several authors. The essential contribution of our former investigation (Ref. 3) is the calculation of the non-equilibrium flow. The throat conditions determined from the equilibrium flow calculation represent the initial values for the non-equilibrium flow in the supersonic portion of the nozzle. In addition, in order to start the numerical integration, the derivatives at the throat had to be specified and they were taken to be those of the equilibrium flow.

In non-equilibrium flow the solution depends on the shape of the nozzle and on its absolute dimensions. Because many hypersonic nozzles are axisymmetric and have an approximately conical shape, the following geometry has been selected:

$$\frac{A}{A^*} = 1 + \left(\frac{x}{f}\right)^2$$

with the parameter

$$f \equiv \frac{d}{2 \tan \chi}$$

where d is the diameter of the throat and χ is the asymptotic angle of the nozzle.

The numerical calculations have been carried out for various values of the parameter f ranging from about 0.9 to 2.0 cm. This covers a family of nozzles with cone angles ranging from 5° to 30°, with throat diameters ranging from 0.15 to 2.0 cm, with total nozzle lengths between 90 and 200 cm and with a maximum area ratio of 10,000.

As the shape of the nozzle is a specified function of x, the above system of differential equations could be simultaneously solved on a high speed computer, the IBM 7090, using the so-called third order Runge-Kutta integration method.

4.3 Numerical Results of Hypersonic Nozzle Flow

The degree of oxygen dissociation α along the hypersonic nozzle is shown in Figure 8 for some characteristic supply pressures and temperatures. Both equilibrium and non-equilibrium flow calculations are shown in the same diagram. For equilibrium flow, the degree of dissociation decreases rapidly due to the strongly decreasing temperature and density. In contrast, non-equilibrium flow shows only small effect of recombination and then freezing of the degree of dissociation α shortly downstream of the throat, at an area ratio of 2 to 5. From there downstream, the degree of the dissociation stays very nearly constant, or stated differently, the chemical composition is practically frozen. At a fixed supply pressure, the degree of dissociation at which the flow freezes increases with increasing supply temperature. At a fixed supply temperature, the frozen dissociation decreases with increasing supply pressure.

The freezing of the chemical composition just downstream of the throat was already observed by Bray (Ref. 18) for Lighthill's "ideally dissociated gas". This can be explained by the fact that dissociation and recombination processes, which are balanced in the reservoir due to equilibrium conditions, decrease at different rates as the air expands. In particular, the rate of dissociation tends to zero first, decreasing strongly with temperature and thereby leaving first the recombination rate as the net reaction, and α decreases. Later, also the recombination rate tends to zero because it is proportional to the square of the density. Hence, $d\alpha/dx$ rapidly approaches zero in the divergent portion of the nozzle, meaning α becomes constant.

The temperature distribution along the hypersonic nozzle is shown in Figure 9 for both equilibrium and non-equilibrium flow for a supply pressure of 50 atm and for various supply temperatures. The temperatures calculated for non-equilibrium flow are much different than those calculated from an assumption of equilibrium. The ratio of equilibrium to non-equilibrium temperature can reach a factor 4 in certain cases. The reason for it is the fact that the energy of dissociation, which is contained in the gas near the throat, is released step by step in equilibrium flow. In contrast, at non-equilibrium flow this energy stays practically frozen in the gas and does not contribute to the temperature. Because no energy is released in the non-equilibrium flow,

this corresponds very closely to an adiabatic expansion of a perfect gas, of course with a different γ than for air at standard condition. The temperature distribution for a perfect gas with $\gamma = 1.4$ has been included for comparison.

The Mach number distribution along the hypersonic nozzle is shown in Figure 10 both for equilibrium and non-equilibrium flow for a supply pressure of 10 atm. Because sound velocity is closely related to temperature, the Mach number distributions show similar strong discrepancies between equilibrium and non-equilibrium flow. The ratio of the Mach numbers between the two cases can reach a factor 1.8. It is noted that the Mach number for a perfect gas with $\gamma = 1.4$ is close to the lines of non-equilibrium Mach numbers. It should be observed that the liberation of the dissociation energy by the recombination process in equilibrium flow defeats markedly the purpose of a hypersonic nozzle, namely to produce high Mach numbers by a certain expansion ratio. For non-equilibrium flow fortunately, this undesired effect has been strongly reduced or cancelled. For most experiments, both a high Mach number and an undissociated free stream are desired, whereas non-equilibrium flow results in a dissociated free stream.

Pressure and density distributions have also been calculated for the same combinations of supply pressure and temperature. They are not presented here. Pressure is affected similarly, but somewhat less than temperature. The ratio between equilibrium and non-equilibrium flow can reach factor 3. The density is very little affected, only up to 15%. Investigation of the effect of the length parameter f, which was varied a factor 2.3, on the flow parameters reveals practically no influence of the nozzle, if the flow parameters are compared at a specified area ratio A/A^*. Only a very small decrease in the degree of dissociation (of about 1%) can be observed comparing the shortest and the longest nozzle, that is the longer nozzle only slightly assists in the recombination process.

5. NON-EQUILIBRIUM FLOW AROUND BLUNT BODIES WITHOUT AND WITH DISSOCIATION IN THE FREE STREAM

5.1 Direct and Inverse Methods for Flow Calculation

The importance of blunted shapes in the hypersonic flight of a vehicle re-entering the atmosphere from outer space has led to many investigations of hypersonic flows with detached shock waves, using both inverse and direct methods. In the inverse method a certain shock shape is assumed or prescribed, and then the governing equations are integrated through the flow field, and the associated body shape follows from the calculation. This method has the advantage that the problems associated with the specification of boundary conditions along an unknown shock wave are avoided. Although it has been successfully applied, for example, by Hall (Ref. 19) even for real gas, the method is extremely tedious if the flow field around a desired body shape has to be determined. In contrast, the investigators at the University of Alabama Research Institute in Huntsville have used a direct method, where the body shape is given and the flow field, including the shock shape, is a result of the calculation. This method uses "integral relations".

In 1959 Dorodnitsyn (Ref. 20) had described this method of integral relations for the solution of two-dimensional boundary value problems. This method is also applicable to problems with free boundaries, such as the shock wave, and has first been applied by Belotserkovskii (Ref. 21) to the calculation of supersonic flow of a perfect gas past a circular cylinder. Also, using a perfect gas, the basic work has been extended by various other authors (Ref. 22, 23, 24) for other body shapes.

Up to the present time, only a limited number of investigators have obtained results for real gas flows in connection with the integral method. The first results were presented by Shih, Baron, e.a. (Ref. 25), for hypersonic non-equilibrium flow of air past a sphere. Simultaneously, Yalamanchili and Hermann (Ref. 3, 26) investigated non-equilibrium flow of air past a circular cylinder for one particular case. Later Belotserkovskii (Ref. 27) used the integral method to calculate equilibrium flow of air past spheres and ellipsoids.

Very recently Hermann and Thoenes (Ref. 28) have given new, extended and improved results for non-equilibrium hypersonic flow of air past a circular cylinder. They have also treated, for the first time to the author's knowledge, the case of dissocia-

tion in the free stream. Such conditions are encountered either in the atmosphere at high altitude (above 90 km), or in the nozzle of modern heated high speed flow facilities designed to simulate re-entry flight conditions, where appreciable frozen dissociation may occur (Section 4.3).

5.2 The Integral Method of Dorodnitsyn and Its Application to the Inviscid Flow Around a Circular Cylinder

5.2.1 Basic Equations

We are restricting ourselves to inviscid flow, and hence we are neglecting viscosity, heat conduction and also radiation. We are using the basic equation of motion for steady adiabatic flow. A polar coordinate system, referred to the center line of the cylinder, is the most suitable one. Figure II shows the cylinder with the radius r_b, the shock wave produced by the flow, the local shock wave angle σ, the local shock wave detachment distance Δ, and the various velocity components before and behind the shock. The transformation of the four conservation equations from the vectorial form to polar coordinates is standard. The results are four partial differential equations:

Conservation of mass:

$$\frac{\partial}{\partial\theta}(\rho u) + \frac{\partial}{\partial r}(\rho v r) = 0 \tag{5.1}$$

θ-momentum:

$$u\frac{\partial u}{\partial\theta} + vr\frac{\partial u}{\partial r} + uv + \frac{1}{\rho}\frac{\partial p}{\partial\theta} = 0 \tag{5.2}$$

r-momentum:

$$\frac{\partial}{\partial\theta}(\rho uv) + \frac{\partial}{\partial r}\left[(p + \rho v^2)r\right] - (p + \rho u^2) = 0 \tag{5.3}$$

Rate equation:

$$u\frac{\partial a}{\partial\theta} + vr\frac{\partial a}{\partial r} - Fr = 0 \tag{5.4}$$

The last equation, expressing the conservation of oxygen atoms, had to be added since the gas under consideration is reacting. F is the source function of oxygen atoms, derived in Section 3.

$$F = \frac{C^2 \rho^2 Z k_d}{2b} \left[\frac{1 - \alpha}{2C\rho} - \frac{\alpha^2}{K_c} \right] \tag{5.5}$$

In order to solve these equations for the unknowns, they must be supplemented by the equation for the conservation of energy, containing an expression for the enthalpy derived in Section 3 (Equ. 3.43).

$$h = R \left[ba D'_{02} + \frac{3}{2} baT + \frac{7}{2} T + (1 - a) \frac{b\theta_{02}}{e^{\theta_{02}/T} - 1} + (1 - b) \frac{\theta_{N2}}{e^{\theta_{N2}/T} - 1} \right] \tag{5.6}$$

and by the thermal equation of state given before (Section 3). Note that the first three equations (conservation of mass and of the two momenta) are independent of the particular gas model, while the last three equations (rate, energy, equation of state) do depend strongly on the particular gas model. The conservation of mass and the r-momentum equation are given in the so-called divergence form, which is required for the application of the integral method.

5.2.2 Boundary Conditions

The condition for flow tangency on the body surface is

$$v_b = 0 \tag{5.7}$$

The conditions behind the shock are obtained from the conservation of mass, momentum and energy across the shock in the conventional way. The parameters across the shock depend considerably on the free stream conditions such as velocity, composition, (for instance, whether free stream dissociation is present or not), and the temperature. In addition, they depend on the way the transition takes place through the shock, i.e., whether the gas is assumed to be in equilibrium or in the frozen state immediately downstream of the shock. For the present non-equilibrium flow calculation, it will be assumed that the chemical composition of the air does not change across the shock, i.e., $a_1 = a_s$. It may be noted that numerical results of the above shock calculation are given for a wide range of free stream conditions in Ref. 29.

Various relations between the velocity components before and after the shock which will be needed later are obtained from Figure 11. The same figure also indicates

that the relation between local dimensionless shock wave distance from the body ϵ and the shock wave angle σ is given by

$$\frac{d\epsilon}{d\theta} = -(1 + \epsilon)\cot(\sigma + \theta) \tag{5.8}$$

where σ and ϵ are functions of θ.

5.2.3 Application of the One-Strip Integral Method

The method of integral relations, proposed by A. A. Dorodnitsyn (Ref. 20), and first applied by Belotserkovskii (Ref. 21), is already well known. Its application to the calculations of hypersonic flow past blunt bodies was also described in Ref. 3 and will not be repeated here. In contrast to the presentation given in Ref. 3, a slight modification of the method, previously used in Ref. 25 and 13, has been applied. It consists of a reduction of the number of equations for which the linear variation, typical for the one-strip integral method, must be assumed.

Due to the boundary conditions (eq. 5.7), it can be seen that the θ-momentum equation and the rate equation may be used in their exact forms. Hence, only two equations of the set, namely the conservation of mass and the r-momentum equation, are approximated by assuming a linear variation of certain integrands across the shock layer. Thus an integration of the equations in the direction of the radial coordinate can be performed, which in turn results in two ordinary differential equations with the tangential coordinate as independent variable. Making use of the boundary condition (eq. 5.7), the complete set of governing equations are as follows:

Continuity:

$$\rho_b \frac{du_b}{d\theta} + u_b \frac{d\rho_b}{d\theta} + \rho_s \frac{du_s}{d\theta} + u_s \frac{d\rho_s}{d\theta} =$$

$$\frac{1 + \epsilon}{\epsilon}\left[(\rho_b u_b - \rho_s u_s)\cot(\sigma + \theta) - 2\rho_s v_s\right] \tag{5.9}$$

θ-momentum:

$$\rho_b u_b \frac{du_b}{d\theta} + \frac{dp_b}{d\theta} = 0 \tag{5.10}$$

r-momentum:

$$\frac{d}{d\theta}(\rho_s u_s v_s) = \frac{2+\epsilon}{\epsilon}(p_b - p_s) + \rho_b u_b^2 + \rho_s u_s^2 - \frac{1+\epsilon}{\epsilon}\left[\rho_s u_s v_s \cot(\sigma+\theta) + 2\rho_s v_s^2\right] \tag{5.11}$$

Rate:

$$u_b \frac{d\alpha_b}{d\theta} = F_b r_b \tag{5.12}$$

Energy:

$$\frac{u_b^2}{2} + h_b = h_t = \frac{u_1^2}{2} + h_1 = \text{constant} \tag{5.13}$$

Equation of State:

$$p_b = \rho_b R Z_b T_b \tag{5.14}$$

These constitute, together with the geometric relation (5.8), a system of seven equations for the seven unknowns. There are four ordinary differential equations and three algebraic equations. The seven unknowns are the five parameters along the wall of the cylinder u_b, ρ_b, p_b, T_b, a_b, and the two parameters for the shock shape, ϵ and σ.

Those equations also contain five variables which are eventually all functions of ρ_b, a_b, T_b. Those are h_b, Z_b, and F_b. F_b is also dependent on k_{db} and K_{cb} which, however, are also functions of T_b and a_b. All those five variables are calculated by subroutines during the process of the solution.

The system of equations also contains velocities, density, and pressure behind the shock, namely u_s, v_s, ρ_s, p_s. They are all functions of free stream Mach number M_1, and shock wave angle σ, and degree of free stream dissociation a_1. They have to be calculated also by special subroutines during the process of the solution.

5.3 Numerical Calculation of the Parameters in the Flow Field Between Shock and Cylinder Surface

5.3.1 Calculation of the Flow Along the Stagnation Streamline and the Stagnation Point Condition

Before the numerical integration of the system of equations for the flow around the circular cylinder can be started, the stagnation point parameters, serving as initial values, must be determined. For this purpose, the governing equations are specialized for the stagnation streamline, where $\theta = 0$ and $u_b = u_s = 0$. The equation for continuity, r-momentum, rate equation, energy equation and equation of state constitute a system of five equations for the five unknowns p, ρ, T, α, and v along the stagnation streamline. After some elimination, the following set of three first-order ordinary differential equations is obtained:

$$\frac{d\alpha}{dr} = \frac{F}{v} \tag{5.15}$$

$$\frac{dT}{dr} = \frac{p\left[v + \left(\frac{\partial u}{\partial \theta}\right)_{\theta=0}\right] - r\rho F\left[RTb - \left(\frac{\partial h}{\partial \alpha}\right)_T (1 - p/\rho v^2)\right]}{r\rho v\left[RZ - \left(\frac{\partial h}{\partial T}\right)_\alpha (1 - p/\rho v^2)\right]} \tag{5.16}$$

$$\frac{d\rho}{dr} = \frac{\rho}{v^2}\left\{\left(\frac{\partial h}{\partial \alpha}\right)_T \frac{F}{v} + \left(\frac{\partial h}{\partial T}\right)_\alpha \frac{dT}{dr} - \frac{v}{r}\left[v + \left(\frac{\partial u}{\partial \theta}\right)_{\theta = 0}\right]\right\} \tag{5.17}$$

Equations (5.16) and (5.17) still contain the unknown gradient of u in θ-direction, which for fixed $\theta = 0$ is a function of the radial coordinate r only. In order to determine this gradient, use is made of the linear approximation for ρu, which was previously needed in order to derive eq. (5.9). After considerable calculation, described in detail in Ref. 28, one finally obtains the expression

$$\left(\frac{\partial u}{\partial \theta}\right)_{\theta=0} = \frac{2\rho_s v_s^2 (1+\epsilon_o)(\eta - 1) + (p_b - p_s)(2+\epsilon_o)\left[\epsilon_o - 2(\eta - 1)\right]}{-\rho v_s \epsilon_o^2} \tag{5.18}$$

Hence, we now have a system (5.15) through (5.17) together with the energy equation, the equation of state and equation (5.18). The system of six equations can be solved for any particular chosen value for ϵ_o, the stagnation point shock detachment distance.

For the solution, a stagnation point pressure p_b must be assumed as a first trial, then the system is integrated and iterated on p_b, until the assumed value p_b agrees with that resulting from the integration.

For both the integration along the stagnation streamline and for the integration along the body surface (described in Section 5.3.2), a fixed-step Runge-Kutta technique of fourth-order accuracy was used. One thousand steps were chosen for the stagnation streamline from the shock to the stagnation point. All calculations were performed on a UNIVAC 1107 high speed digital computer, which is located in the University of Alabama Research Institute.

5.3.2 Calculation of the Flow Variables Along the Cylinder Surface and Behind the Shock

After the stagnation point conditions have been obtained, as described in Section 5.3.1 , the integration around the body is started with an unknown, but assumed shock detachment distance ϵ_o, which must be iterated. The integration is done by the same technique and on the same computer as described in Section 5.3.1. The step size was fixed at 0.002 radians, and approximately 800 steps were used for the integration from the stagnation point to the equator ($\theta = \pi/2$). The equations for the variables along the cylinder surface are strongly dependent on the selected value ϵ_o, and smooth transitions of all variables from the subsonic to the supersonic flow regime are only obtained for a correctly chosen ϵ_o. Depending on the case, between ten and fifteen iterations were needed to determine ϵ_o to four significant figures. Near the point where the surface velocity reaches the local speed of sound, the equations have a singularity. For the cases of frozen and equilibrium flow, the singularity occurs at the sonic point; however, this is not true for non-equilibrium flow (Ref. 25). Previous investigators (Ref. 21, 25, 27) have reported that the singularity is of the saddle point type. In the present formulation of the problem, this was not apparent, and more research in this direction seems to be necessary.

Once a smooth distribution of all variables in the entire subsonic region was obtained, all dependent variables were extrapolated into the supersonic region by using a second -order polynomial curve fit. The integration was then resumed and could, in most cases, be carried out to the equator of the body, and in some cases even farther.

5.4 Discussion of the Results of the Flow Around a Cylinder

5.4.1 Flow Along the Stagnation Streamline

Numerical results have been obtained for a number of cases, only a few of which can be discussed here. For chemical non-equilibrium flow, the degree of dissociation and the temperature are particularly interesting parameters. Fig. 12 and 13 show the distribution of α and T along the stagnation streamline behind the bow shock for a flight speed of 4300 m/sec at an altitude of 30 km. Note that with $T_1 = 225^\circ K$, the temperature scale goes from $4500^\circ K$ to $7650^\circ K$. That means the non-equilibrium temperature existing behind the shock for small bodies is about $3000^\circ K$ higher than the equilibrium temperature existing for large bodies. It can be seen that, depending on the size of the body, quite different regimes of non-equilibrium flow are encountered. For relatively large bodies, a characteristic flow time is large compared to the local chemical relaxation time, which causes the flow to reach the state of thermodynamic equilibrium close behind the shock. On the other hand, for very small bodies, a characteristic flow time is very short if compared to the relaxation time. In this case, the flow remains essentially frozen and equilibrates only near the stagnation point, where the velocity approaches zero and the local residence time of a flow particle again is large compared to the relaxation time. It was found that the flow always reaches thermodynamic equilibrium at the stagnation point.

In both figures the present results from the integral method are compared with data calculated by Conti (Ref. 30), who used an inverse method, also a basically different approach, and somewhat different reaction rate constants. The air model was the same as ours. The comparison is very gratifying.

5.4.2 Flow Around Circular Cylinder

It is already well known from perfect gas calculations that with increasing free stream Mach numbers the bow shock moves closer to the body. It is seen from Fig. 14 and 15 that in chemical non-equilibrium flow this trend is retained. Both figures also indicate clearly that dissociation of the free stream, keeping all other free stream parameters unchanged, causes the bow shock to move away from the body. One reason for this effect is that, for a dissociated free stream, the density behind the shock is lower than for corresponding conditions without free stream dissociation (Ref. 29).

The effect is seen to increase with decreasing free stream Mach number. Fig. 14 also shows that the shock shape deviates considerably from a concentric circle, even where the velocity in the shock layer is still subsonic.

From Fig. 15 it is observed that the present calculations yield a stagnation shock detachment distance which is much smaller, even for an undissociated free stream, than the values obtained from perfect gas calculations (Ref. 21, 24). It should be noted that the calculations for perfect gas by Archer, who used a one-strip solution, agrees excellently with the one by Belotserkovskii, who used a three-strip solution. This indicates that for this type of calculation, a one-strip solution yields very satisfactory accuracy. It is important to see that for a free stream Mach number of $M_1 = 3$, where the bow shock does not yet cause appreciable molecular vibration in the shock layer, the present calculation furnishes a value which is very close to the known perfect gas results. Responsible for the effect that shock detachment distance of the present calculation yields smaller values than that for the perfect gas at Mach numbers approximately 4 to 7, is that our calculations included the energy of molecular vibration. For Mach number 6.8, the present calculation, which includes dissociation, does not show any degree of dissociation in the flow field (Fig. 17). Hence, the difference between the present calculation and the perfect gas calculation must be the inclusion of the molecular vibration energy in our calculations. Of course beyond Mach number 7, the influence of the dissociation on the shock detachment distance will become more and more pronounced. Again, it is gratifying to see that for the high Mach number range ($M_1 = 14.2$) our results agree closely with those of Conti (Ref. 30), which were obtained by an entirely different approach. It must be mentioned here that numerical results from our previous investigation (Ref. 3) as reported for one particular case ($M = 14$; $\alpha_1 = 0.7$) were found to be incorrect due to an error in the computer program. However, all equations are correct as published.

The velocity distribution along the surface of the cylinder as evident from Fig. 16 is almost linear up to the sonic point. A distinct effect of free stream dissociation can be seen.

The degree of oxygen dissociation along the non-catalytic body surface is presented in Fig. 17. For zero free stream dissociation, it is seen that at $M_1 = 6.6$

no dissociation occurs along the body. The degree of dissociation increases strongly with increasing Mach number and reaches about 0.95 at Mach number 14.2. Especially for the high Mach number cases, it is seen that the recombination process dominates in the subsonic regime as the flow expands around the body. The degree of dissociation decreases slowly until, in the supersonic regime, the local residence time of a particle becomes so small compared to the relaxation time that the flow freezes. With lower free stream Mach numbers, this effect becomes less pronounced until, for the lowest case shown, no change in composition at all is observed. For a better understanding, however, the non-equilibrium results should be compared to those for equilibrium flow and frozen flow, which are not available at the present time.

Finally, Fig. 18 and 19 show the temperature and the pressure distribution along the surface of the cylinder for selected free stream Mach numbers with and without dissociation of the free stream. As expected, free stream dissociation has a strong effect on the temperature but practically no effect on the pressure. Therefore, pressure distributions are presented only for zero free stream dissociation. Note that for $M_1 = 6.6$ the presence of free stream dissociation raises the stagnation temperature about 1000 °K.

5.5 Comparison with Flow Around a Sphere

So far, a large number of data have been presented for the circular cylinder. There is no doubt that from an engineering point of view, the sphere or the spherically capped cone has a greater interest. However, only a restricted number of data for the sphere are available for non-equilibrium flow, including dissociation (Ref. 25). Figure 20 shows a comparison of the shock detachment distance between the cylinder and sphere with the results from the sphere taken from Ref. 25. Note that the Mach number is nearly identical; the altitude, however, is markedly different. Both are valid for zero free stream dissociation. It is seen that the shock wave for the sphere is much closer to the body and has less than one half of the distance of the shock wave for the cylinder. Results with exact equal free stream conditions for both cases are not available at the present time. The fact that the shock wave of the sphere is much closer to the body than for the cylinder should be true also for identical free stream conditions. It is known to be the case for supersonic flow of a perfect gas. Note that the location of the sonic point is very sensitive to free stream conditions, thus one cannot compare sonic point locations of two bodies with different free stream conditions.

6. NON-EQUILIBRIUM FLOW AROUND A POINTED CONE WITHOUT AND WITH DISSOCIATION IN THE FREE STREAM

6.1 Review of Cone Flow Calculations for Real Gases

Over the past few years considerable effort has been devoted to the hypersonic blunt body problem using both inverse and direct calculation techniques (See Section 5.). Comparatively less interest has been paid to the high temperature real gas flow past pointed bodies, which presently appears to be of growing interest.

In order to solve the problem of supersonic flow past any body, the conditions behind the shock wave should be available for use as initial or boundary conditions, depending on whether the governing equations are solved by integrating from the assumed shock wave toward the unknown body (the inverse method), or from the known body towards the unknown shock (the direct method).

The classical example of supersonic pointed body flow is flow past an infinite circular cone at zero angle of attack. The principle of conical supersonic flow, that all parameters are constant on co-axial conical surfaces, was first conceived by A. Busemann in 1928. For supersonic perfect gas flow, the parameters then are independent of distance from the apex of the cone, and depend only on the polar angle. Hence, the flow parameters are described by a system of ordinary, non-linear differential equations. Those differential equations, often referred to as the Taylor-Maccoll equations, cannot be solved in closed form. They were solved numerically first by Taylor and Maccoll. An extended machine solution was given by Kopal in 1947, for a perfect gas and supersonic flow. Much later Melnik (Ref. 31) used Dorodnitsyn's method of integral relations to calculate supersonic and hypersonic flow of a perfect gas about elliptical cones.

Real gas effects were considered first by Feldman (Ref. 32) in 1957 for dissociated air in equilibrium, however, with very simplifying assumptions. Later Romig (Ref. 33, 34) gave a numerical integration of the Taylor-Maccoll equation for equilibrium flow of air, using tabulated thermodynamic data. Sedney and Gerber (Ref. 35) calculated vibrational non-equilibrium flow over a cone using the method of characteristics. Recently Capiaux and Washington (Ref. 36) treated non-equilibrium flow of an "ideal dissociating gas" (so-called Lighthill's gas) past a wedge, not a cone,

also using the method of characteristics. The first application of Dorodnitsyn's integral method to the real gas flow past pointed cones was given by South (Ref. 37). He considered vibrationally relaxing flow of a pure diatomic gas, but did not consider dissociation.

The application of the method of integral relations to the problem of hypersonic flow of air with non-equilibrium dissociation past a pointed cone was first presented, to our knowledge, by J. Thoenes (Ref. 13) and in Section 6 we will closely follow his presentation. It can be shown that for a large range of velocities, altitudes, and cone angles, an appreciable degree of oxygen dissociation behind the attached shock is found, but nitrogen dissociation need not be considered as long as the boundary layer is disregarded. Hence, his investigation uses the same simplified air model, consisting of the three components O, O_2, and N_2 only, which was used in Sections 3, 4, and 5.

6.2 Basic Equations for the Flow Around a Sharp Biconvex Twodimensional and a Pointed Axisymmetric Body

We start from the basic equations of steady adiabatic flow, neglecting viscosity, heat conduction, and radiation in the same way as we did in Section 5. The equation of state and the energy equation are the same and are not repeated here. We transform the vector equation to an orthogonal curvilinear coordinate system with coordinates tangential and normal to the body surface. The equations are valid for plane flow (with $j=0$) and axisymmetric flow (with $j=1$). Fig. 21 shows the coordinate system and shock geometry, of an arbitrary pointed body of revolution. Note that the radius of curvature, R, is a function of x. In the equation, the curvature itself, K(x), is used. We are restricting ourselves to symmetric flow, that is no angle of attack. The resulting equations are as follows:

Conservation of mass:

$$\frac{\partial}{\partial x}\left(\rho u r^j\right) + \frac{\partial}{\partial y}\left[(1 + Ky)\,\rho v r^j\right] = 0 \qquad (6.1)$$

The equation for the x-momentum, y-momentum, and rate equation are not written in the usual form but transformed immediately to the "divergence form" which is required for the application of the integral method.

x-momentum:

$$\frac{\partial}{\partial x}\left[(p + \rho u^2) r^j\right] + \frac{\partial}{\partial y}\left[(1 + Ky)\rho uv r^j\right]$$

$$+ \rho uv r^j K - jp\left[\frac{dr_b}{dx} - y \sin\theta \frac{d\theta}{dx}\right] = 0 \qquad (6.2)$$

y-momentum:

$$\frac{\partial}{\partial x}(\rho uv r^j) + \frac{\partial}{\partial y}\left[(1 + Ky)(p + \rho v^2) r^j\right]$$

$$- (p + \rho u^2) K r^j - jp (1 + Ky)\cos\theta = 0 \qquad (6.3)$$

rate equation:

$$\frac{\partial}{\partial x}(\rho u \alpha r^j) + \frac{\partial}{\partial y}\left[(1 + Ky)\rho v \alpha r^j\right] - \rho r^j F(1 + Ky) = 0 \qquad (6.4)$$

The boundary conditions are very similar to those outlined in Section 5.2.2 for the blunt body. In particular, the condition for flow tangency at the body surface is given by:

$$v_b = 0 \qquad (6.5)$$

The assumption of frozen chemical composition across the shock and hence the conditions behind the shock are the same, as in 5.22. We will later present one result on equilibrium calculation for cone flow. For this, of course, equilibrium condition across the shock was taken as a boundary condition.

There are also velocity relations across the shock, equivalent to those of the blunt body, explained in Section 5.2.2. Also, Figure 21 indicates the relation between the shock coordinate y_s and shock wave angle σ as:

$$\frac{dy_s}{dx} = (1 + Ky_s) \tan(\sigma - \theta) \qquad (6.6)$$

where, in general, σ and θ are functions of x.

6.3 Application of the One-Strip Integral Method for the Flow Calculation Around A Pointed Cone

We apply the method of integral relations as described by Dorodnitsyn (Ref. 20) to the partial differential equations which were written in divergence form (6.1, 6.2, 6.3, 6.4). We use the method in its simplest form with one-strip, which is equivalent to a first order or linear approximation of certain groups of the variables along the y coordinate. After considerable calculations the system of ordinary differential equations (6.7 thru 6.12) is obtained. They are valid along the shock and along the body surface. The subscript b refers to conditions at body surface, while the subscript s as in ρ_s, u_s, v_s, p_s refers to the conditions behind the shock.

Continuity:

$$\rho_b r_b^i \frac{du_b}{dx} + u_b r_b^i \frac{d\rho_b}{dx} + i\,\rho_b u_b \frac{dr_b}{dx} + \rho_s r_s^i \frac{du_s}{dx} + u_s r_s^i \frac{d\rho_s}{dx} + i\,\rho_s u_s \frac{dr_s}{dx}$$

$$= \frac{1}{y_s}\left(\rho_s u_s r_s^i - \rho_b u_b r_b^i\right)\frac{dy_s}{dx} - \frac{2}{y_s}\left(1 + Ky_s\right)\rho_s v_s r_s^i \qquad (6.7)$$

x-momentum:

$$2\rho_b u_b r_b^i \frac{du_b}{dx} + u_b^2 r_b^i \frac{d\rho_b}{dx} + r_b^i \frac{dp_b}{dx} + i\left(\rho_b u_b^2 - p_s\right)\frac{dr_b}{dx}$$

$$+ 2\rho_s u_s r_s^i \frac{du_s}{dx} + u_s^2 r_s^i \frac{d\rho_s}{dx} + r_s^i \frac{dp_s}{dx} + i\left(p_s + \rho_s u_s^2\right)\frac{dr_s}{dx} = \frac{1}{y_s}\left[\left(p_s + \rho_s u_s^2\right) r_s^i\right.$$

$$\left. - \left(p_b + \rho_b u_b^2\right) r_b^i\right]\frac{dy_s}{dx} - \rho_s u_s v_s r_s^i \left(3K + \frac{2}{y_s}\right) - i p_s y_s \sin\theta \frac{d\theta}{dx} \qquad (6.8)$$

y-momentum:

$$u_s v_s r_s^i \frac{d\rho_s}{dx} + \rho_s v_s r_s^i \frac{du_s}{dx} + \rho_s u_s r_s^i \frac{dv_s}{dx} + i\,\rho_s u_s v_s \frac{dr_s}{dx} = \frac{1}{y_s}\left(\rho_s u_s v_s r_s^i\right)\frac{dy_s}{dx}$$

$$- \frac{2}{y_s}\left[\left(1 + Ky_s\right)\left(p_s + \rho_s v_s^2\right) r_s^i - p_b r_b^i\right]$$

$$+ K\left[\left(p_s + \rho_s u_s^2\right) r_s^i + \left(p_b + \rho_b u_b^2\right) r_b^i\right] + i\cos\theta\left[p_s\left(1 + Ky_s\right) + p_b\right] \qquad (6.9)$$

Rate:

$$\rho_b a_b r_b^j \frac{du_b}{dx} + u_b a_b r_b^j \frac{d\rho_b}{dx} + \rho_b u_b r_b^j \frac{da_b}{dx} + j\rho_b u_b a_b \frac{dr_b}{dx}$$

$$+ \rho_s a_s r_s^j \frac{du_s}{dx} + u_s a_s r_s^j \frac{d\rho_s}{dx} + \rho_s u_s r_s^j \frac{da_s}{dx} + j\rho_s u_s a_s \frac{dr_s}{dx} =$$

$$= \frac{1}{y_s} [\rho_s u_s a_s r_s^j - \rho_b u_b a_b r_b^j] \frac{dy_s}{dx} + (1 + Ky_s)(F_s - \frac{2}{y_s} v_s a_s)\rho_s r_s^j + \rho_b r_b^j F_b \qquad (6.10)$$

Energy:

$$h_b + \frac{1}{2} u_b^2 = h_t = \text{constant} \qquad (6.11)$$

State:

$$p_b = \rho_b RZ_b T_b \qquad (6.12)$$

The first three equations express conservation of mass and momenta independent of the gas model. The rate equation expresses the non-equilibrium aspects of the flow under consideration. This equation, together with the equation of energy and the equation of state pertain to the specific gas model being applied here. Together with the geometric relation (6.6) these constitute seven equations for the seven unknowns: u_b, p_b, ρ_b, T_b, and a_b, plus the shock parameters, σ the shock angle, and y_s the distance of the shock from the cone surface. The dissociation and recombination rate constants enter in the source function F which is therefore a function of α, ρ, and T. The enthalpy h is also a function of α and T.

The parameters behind the shock (with subscript s) have not been determined yet. They must be calculated for each point along the shock, assuming either frozen or equilibrium composition downstream of the shock.

6.3.1 Frozen Flow Around a Cone

We are considering from now on flow around a cone. Hence we have to specialize all equations above for $j = 1$ and $K = 0$. For a perfect gas, the observation

of straight shock waves and constant surface pressure in the conical flow field confirms the original concept of conical flow, that there is no length scale.

A frozen flow behaves like a perfect gas flow, only with a different chemical composition and therefore a different ratio of specific heats, γ. South (37) has used these facts of a straight shock wave and constant properties along the cone surface and shock surface to simplify the first approximation equations derived above. By the same procedure, it was found that, although the rate equation (6.10) is meaningless, equations 6.7 through 6.9 reduce to simple algebraic equations as follows.

Continuity:

$$\rho_b u_b + \rho_s v_s \left[\cot(\sigma - \theta) + \cot\theta\right] = 0 \qquad (6.13)$$

x-momentum:

$$2\rho_b u_b^2 + 2\left[\cot(\sigma - \theta) + \cot\theta\right] \rho_s u_s v_s + (p_b - p_s) = 0 \qquad (6.14)$$

y-momentum:

$$2\left[\cot\theta + \cot(\sigma - \theta)\right] \rho_s v_s^2 - \left[\cot\theta + 2\cot(\sigma - \theta)\right](p_b - p_s) = 0 \qquad (6.15)$$

Elimination of $(p_b - p_s)$ from the last two equations, and using the continuity equation, furnishes

$$u_b = u_s + \frac{v_s}{\cot\theta + 2\cot(\sigma - \theta)} \qquad (6.16)$$

and subsequently all the other variables on the body surface in terms of the values behind the shock. Equations 6.13, to 6.15, together with the energy equation (6.11) and the equation of state (6.12), then represent five equations for the five unknowns u_b, ρ_b, T_b, p_b, and σ. Specifying α_1 and cone angle θ, we can calculate chemically frozen cone flow with the molecular vibrations either frozen, or in equilibrium with the translational and rotational energy. By assuming $\alpha_1 = 0$ and a low free stream temperature, and by considering the molecular vibration frozen at the free stream value, all the parameters obtained were in very good agreement with the well known perfect gas results ($\gamma = 1.4$).

6.3.2 Equilibrium Flow Around a Cone

The same considerations as were pointed out above on frozen flow apply for the case of chemical equilibrium flow, i.e., there is also no length scale, and hence all parameters must be constant along lines through the apex of the cone.

Newman (Ref. 38) has used equations (6.13) through (6.16) in connection with approximated thermodynamic data from tables to calculate conical flow parameters for air in thermodynamic equilibrium. Thoenes (Ref. 13) used the equilibrium relation as presented in equation (3.19). Equations (6.13) through (6.15), the energy equation (6.11), the equation of state (6.12), and the equilibrium equation (3.19) then constitute a system of six equations for the unknowns u_b, ρ_b, T_b, p_b, a_b, and σ. The specification of the cone angle θ allows the complete solution of the problem. The actual numerical computation proceeds in a similar fashion as for the frozen flow.

6.3.3 The General Case of Non-Equilibrium Flow Around a Cone

In the case of non-equilibrium flow past a cone, no definite statement can be made about the shock shape or the behavior of other flow parameters. As was shown in Section 2.1., any non-equilibrium flow will be non-similar. Hence we cannot expect the flow field to be conical in the sense that the parameters are constant along lines through the apex, or that the shock is a straight cone. All variables must be calculated by integrating the conservation equations, together with the equation of state, in a step-by-step fashion along the length of the cone. For a supersonic flow field, which is considered here, the equations are of hyperbolic character and thus form an initial value problem. Initial values are given by the frozen flow solution, and also the initial gradients can be derived as functions of the initial flow parameters only.

The author used a method he referred to as "the semi-exact procedure", using the x-momentum equation (6.2), the rate equation (6.4) in their exact form, and in addition the continuity equation (6.7) and the y-momentum equation (6.9) in their approximate form. Hence, this set contains only two approximated equations in contrast to the ordinary standard procedure of the integral method, where all four

equations are approximated. Due to the boundary condition, eq. (6.5), it can be seen from eq. (6.2) and (6.4) prior to their being written in the divergence form, that they may be used in their exact forms, leaving, as mentioned, only the continuity (6.7) and the y-momentum eq. (6.9) as approximations.

Consequently, the following set of equations is obtained from the eq. (6.7), (6.2), (6.9), (6.4), (6.11), (6.12), respectively.

Continuity:

$$\rho_b r_b \frac{du_b}{dx} + u_b r_b \frac{d\rho_b}{dx} + \rho_b u_b \frac{dr_b}{dx} + \rho_s r_s \frac{du_s}{dx} + u_s r_s \frac{d\rho_s}{dx} + \rho_s u_s \frac{dr_s}{dx} =$$

$$\frac{1}{y_s} (\rho_s u_s r_s - \rho_b u_b r_b) \frac{dy_s}{dx} - \frac{2}{y_s} \rho_s v_s r_s \qquad (6.17)$$

x-momentum:

$$\rho_b u_b \frac{du_b}{dx} + \frac{dp_b}{dx} = 0 \qquad (6.18)$$

y-momentum:

$$u_s v_s r_s \frac{d\rho_s}{dx} + \rho_s v_s r_s \frac{du_s}{dx} + \rho_s u_s r_s \frac{dv_s}{dx} + \rho_s u_s v_s \frac{dr_s}{dx} =$$

$$\frac{1}{y_s} (\rho_s u_s v_s r_s) \frac{dy_s}{dx} - \frac{2}{y_s} [(p_s + \rho_s v_s^2) r_s - p_b r_b] + (p_s + p_b) \cos\theta \qquad (6.19)$$

Rate:

$$u_b \frac{da_b}{dx} = F_b \qquad (6.20)$$

Energy:

$$h_b + \frac{1}{2} u_b^2 = h_t \qquad (6.21)$$

State:

$$p_b = \rho_b R Z_b T_b \qquad (6.22)$$

Those are 6 equations for the 6 unknowns u_b, ρ_b, T_b, ρ_b, a_b along the body surface and y_s, the shockwave distance from the cone surface as explained before. h_b and F_b are known functions of ρ, T, a. The cone angle θ must be given.

In order to start the numerical integration of system (6.17) through (6.22), the initial values and the initial derivatives of all parameters must be known at the cone tip, $x = 0$. The use of frozen shock conditions implies that the flow is frozen at the tip of the cone; therefore, the frozen flow values serve as initial values. When trying to solve for the derivatives however, indeterminate values occur at $x = 0$. The derivatives are successfully obtained by applying L'Hospital's rule.

6.4 Presentation of the Results

6.4.1 Numerical Technique

For the numerical evaluation and presentation, all variables and coordinates were made dimensionless as follows. The velocity components, pressure, density, and temperature were made dimensionless by the free steam velocity, free steam momentum flow $(\rho_1 u_1^2)$, free stream density, and free stream temperature, respectively. The coordinates x and y were made dimensionless by a characteristic length l defined by

$$l = \left(\frac{u_b}{F_b} \right)_{x=0} \tag{6.23}$$

Here the reciprocal value of F_b represents a characteristic relaxation time. For the cases presented, it is on the order of $4 \cdot 10^{-3}$ sec.

The equations were then programmed in dimensionless form. All calculations were performed on the UNIVAC 1107 computer located at the University of Alabama Research Institute.

For frozen flow and equilibrium flow, the procedure is rather straight forward. For chemical non-equilibrium flow, basically a fixed step Runge-Kutta integration technique of fourth-order accuracy was used. The main program uses essentially four subroutines; one for evaluating the thermodynamic functions, one for the coefficients of the set of equations, one for solving the system of linear equations for the derivatives, and the Runge-Kutta technique for the integration.

6.4.2 Frozen Flow Results

The calculation of the frozen flow was necessary not only in order to obtain initial conditions for the case of chemical non-equilibrium flow, but also for use as an easy check of the system by calculation of cases at relatively low temperatures. The results, not illustrated here, show that the shock wave angle, surface velocity, and surface pressure respectively, obtained with the one-strip integral method for undissociated, fully frozen flow of air, are in full agreement with the exact results of the perfect gas, as it should be. Apparently, for hypersonic conical flow, where the shock wave attaches closely to the cone in the shock layer, the flow variables undergo only slight changes in the direction normal to the body surface; and therefore, the one-strip (linear) approximation is quite adequate.

The influence of free stream dissociation on the angular shock layer thickness for chemically frozen flow is shown in Fig. 22. It indicates that the thickness increases with increasing free stream dissociation. Repeating the calculation with vibrational equilibrium, instead of the frozen vibration, results in a smaller shock angle, particularly at higher free stream velocities and larger cone angles (not shown here). Free stream dissociation increases the surface pressure, and for complete free stream oxygen dissociation and a semivertex angle of $\theta = 10^{\circ}$ at Mach number 5, this increase amounts to about 11%. Under the same conditions, the surface density decreases about 10%. Frozen dissociation has little influence on the surface temperature (not shown in the presented graphs).

6.4.3 Equilibrium Flow Results

Conical flow parameters for thermodynamic equilibrium have been calculated by Thoenes (Ref. 13) in order to demonstrate the validity of the simplified three component air model for the range of cone angles and free stream conditions which were considered. Also, in order to judge the results of the non-equilibrium flow calculations, consistent asymptotic equilibrium values are needed. They have been compared with, what may be called exact, results by Romig (Ref. 34), which were calculated using Taylor-Maccoll's equations in connection with thermodynamic tables. It is rather gratifying to see that the velocity, the pressure, and the temperature on the cone surface are practically identical with the exact values. The shock wave

angle and compressibility factor are somewhat higher, the surface density somewhat lower than the exact value. However, the deviation in no case exceeds 2%. Hence, for this investigation, the assumed gas model is shown to be a very good approximation to atmospheric air. Because of this consistent agreement, no detailed figures with equilibrium results are shown here (except Fig. 26).

6.4.4 Non-Equilibrium Flow Results

Some results for chemical non-equilibrium flow are presented in Figs. 23 thru 26. The case given in these figures for zero free stream dissociation corresponds to a flight Mach number of $M_1 = 20$ at 40 km geometric altitude. For the second case discussed, the free stream dissociation was arbitrarily taken to be $a_1 = 0.5$, leaving all other free stream conditions unchanged. All variables in figures 23 thru 26 are plotted versus the dimensionless distance along the cone surface. The asymptotic equilibrium values indicated in all figures represent the results from the equilibrium flow calculations, (Section 6.7.3) which are based on the assumption of a conical shock wave. It is also noted that free stream dissociation affects finite rate non-equilibrium flow. It should be mentioned that the free stream dissociation and the resulting higher degree of dissociation in the shock layer causes the flow to relax faster, i.e., the respective equilibrium state is reached closer to the tip than in the case of zero free stream dissociation.

The shock wave angle (not shown here) starts first with the frozen value, then decreases, and then afterwards increases a little. However, all those changes are within 0.1 or 0.2 degrees. Surface velocity approaches the asymptotic equilibrium value very closely (within 0.7%). The surface pressure (Fig. 23) is clearly the variable which is the least sensitive to relaxation effects. After a slight overexpansion, the asymptotic equilibrium values are approached within less than 0.1%. Note that all pressure changes are very small. The surface density (Fig. 24) is seen to increase along the body, and it approaches the asymptotic equilibrium value from below. The free stream dissociation reduces the density markedly. The surface temperature also plotted in Figure 24, decreases rapidly away from the tip. Free stream dissociation results in higher temperature. This behavior is, of course, closely related to that of

the degree of dissociation, α, which is shown in Fig. 25. The graph illustrates the usefulness of the x-coordinate made dimensionless with the characteristic relaxation length l. After $\xi = 2$ or 3 for the case of zero free stream dissociation, the flow field dissociation is approximately in equilibrium (horizontal slope). For the case with free stream dissociation $\alpha_1 = 0.5$ the value is already reached at $\xi = 0.5$. It can be seen that the initial gradient of the α versus ξ curve at $\xi = 0$ would reach $\alpha = 1$ at $\xi = 1$ as it should according to the definition of ξ, using l. Fig. 26 finally brings the comparison between the shock layer thickness for non-equilibrium flow compared with the two-limits of a frozen and equilibrium flow. The fact that the much more complex calculation of the non-equilibrium flow produces a shock which is clearly bracketed by the frozen value, from which it starts, and the equilibrium value is very gratifying. It is noted that the shock wave angle slowly approaches the angle for equilibrium flow.

Concluding the discussion of the results, we can state that the free stream dissociation and chemical relaxation in the shock layer have a significant influence on the behavior of most flow variables. Free stream dissociation is known to occur in high temperature gasdynamic flow facilities; and it is, therefore, important to recognize its effects when evaluating experiments performed in such facilities.

7. SUMMARY

The salient features of theoretical hypersonic flow research, including the underlying thermodynamic relations, carried out by the author and his co-workers over the past four years, and some numerical results obtained are reported.

The meaning of equilibrium, non-equilibrium, and frozen flow are discussed. Non-equilibrium flow fields generally are not similar for geometrically similar bodies. The flight regions and the equilibrium values of temperature, pressure, and density, which occur behind the normal shock of a vehicle re-entering the earth's atmosphere from a circular orbit or from a lunar mission, are presented.

Real gas effects are treated using a simplified air model. The pressure equilibrium constants for oxygen and nitrogen dissociation are derived, and explicit equations for the degree of oxygen and nitrogen dissociation in equilibrium are given. The thermal equation of state, the thermodynamic properties of energy and enthalpy, and the rate equation for the net production of oxygen atoms are derived in some detail.

A simplified gas model valid in the range of oxygen dissociation is used to numerically calculate the inviscid flow through hypersonic nozzles, and, by the direct one-strip integral method of Dorodnitsyn, the inviscid flow about the forward portions of blunt bodies (up to the equator), and of pointed cones. Cases of equilibrium, non-equilibrium, and frozen flow, with and without free stream dissociation, are presented. The effects of the absolute size of a blunt body and the absolute length of a cone are investigated.

Some specific results pertaining to a blunt body (nose radius = 10 cm) flying at 30 km altitude are:

(1) Real gas effects can be detected beginning at $M = 3$ due to molecular vibration, and beyond $M = 8$ due to molecular vibration and dissociation. Dissociation of oxygen only occurs in the range between Mach numbers 8 and 14, approximately, while, at higher Mach numbers, nitrogen dissociation must be considered. (2) The shock detachment distance in case of a real gas with an undissociated free stream is much smaller than in case of a perfect gas. (3) Free stream dissociation causes the bow shock to move away from the body. (4) For very small bodies (nose radius < 0.1 cm), and at $M = 14$, the non-equilibrium temperature in the main part of the shock layer near the stagnation streamline is about 3000°K higher than the equilibrium temperature which exists for a sufficiently large body (nose radius = 10 cm).

Some results pertaining to a circular cone with attached shock are:

(1) For a large range of Mach numbers (up to $M = 20$) and cone semivertex angles (up to $\theta = 40^{\circ}$) at 40 km altitude, an appreciable degree of oxygen dissociation is found in the flow field between shock and body, but nitrogen dissociation can be disregarded. (2) For non-equilibrium flow, free stream dissociation markedly decreases the density along the body, results in substantially higher temperature, slightly increases the shock angle, and has little effect on surface pressure. The equilibrium flow results for a cone agree within 2% with the values given by Romig. (3) For non-equilibrium flow, the shock wave of the cone is curved and is bracketed by the location of the frozen shock wave on the outside, and by the position of the equilibrium shock wave which is closer to the body.

8. LIST OF SYMBOLS

A, A^*	Area, Throat Area
b	Constant, defined by Eq. (3.3)
C	Number of oxygen atoms per unit mass of gas
D, D^+	Dissociation energy [J/kmol] and [J/kg], respectively
D'	Characteristic temperature of dissociation [^oK]
e, E	Internal energy [J/kg] or [J/kmol]
E_d	Activation energy of dissociation [J/kmol]
f_i	Mole fractions
F	Source function for oxygen atoms. Eq. (5.5)
g_i	Degeneracy factor
h	Enthalpy [J/kg], also Planck's constant [J • sec]
h_t	Total enthalpy [J/kg]
I	Moment of Inertia
i	Coordinate designator
k	Boltzmann's constant
k_d	Dissociation rate constant [m^3/particle • sec]
k_r	Recombination rate constant [m^6/particle^2 . sec]
K	Curvature
K_c	Concentration equilibrium constant [particles/m^3]
K_p	Pressure equilibrium constant [N/m^3]
l	Characteristic length [m]
$\dot{m}$	Mass flow [kg/sec]
m_i	Mass of one particle of ith species
M	Molecular weight of undissociated gas, also Mach number
M_a	Molecular weight of dissociated gas
M_i	Molecular weight of ith species
n_i	Number of particles of ith species per unit volume (undissociated gas)
$\bar{n}_i$	Number of particles of ith species per unit volume (dissociated gas)
N	Nitrogen

N_A	Avogardro's number [$kmol^{-1}$]
O	Oxygen
p	Pressure [N/m^2]
Q	Partition function
q	Heat addition [J/kg]
$\vec{q}$	Velocity vector
r, θ	Radial and angular coordinates
R	Gas constant of undissociated gas [J/kg ^oK]
R*	Universal gas constant [J/kmol ^oK]
t	Time [sec]
T	Temperature [^oK]
u,v	Velocity components in x, y direction, respectively [m/sec]
w	Net rate of production of oxygen atoms per unit volume of gas
x, y	Coordinates
x	Distance along axis downstream from nozzle throat
Z	Compressibility factor
α	Degree of oxygen dissociation
β	Degree of nitrogen dissociation
γ	Ratio of specific heats
Δ	Local shockwave detachment distance [m]
ϵ	Dimensionless shockwave distance from body
η	Dimensionless radial coordinate, r/r_b
θ	Characteristic vibrational temperature [^oK], and body contour angle
θ_r	Characteristic rotational temperature [^oK]
$\varkappa$	Symmetry Number
ν_i	Stoichiometric coefficient for ith species
ρ	Density [kg/m^3]
σ	Oblique shock angle

Subscripts

1	Free stream
b	Body surface
s	Behind the shock
n	Normal component
t	Tangential component, also total conditions
M	Third-body particle
N2	Molecular nitrogen
N	Atomic nitrogen
O2	Molecular oxygen
O	Atomic oxygen
α	Pertaining to oxygen dissociation
β	Pertaining to nitrogen dissociation
o	Standard conditions

9. REFERENCES

1. Herman, R., "Hypersonic Aerodynamic Problems at Re-Entry of Space Vehicles," Invited lecture presented at the 4. Space Symposium at the University of Goettingen, Germany, Oct. 18-22, 1965. Also University of Alabama Research Institute, Huntsville, UARI Research Report No. 29, November 1965.

2. Hermann, R., "Hypersonic Flow Problems During Re-Entry Into the Atmosphere," Yearbook 1961, Wissenschaftliche Gesellschaft fuer Luftfahrt, Friedr. Vieweg & Sohn, Braunschweig, Germany, 1961.

3. Hermann, R., Yalamanchili, J., "Hypersonic Flow With Non-Equilibrium Dissociation Around Blunt Bodies in Flow Facilities and in Free Flight," Yearbook 1963, Wissenschaftliche Gesellschaft fuer Luftfahrt, Friedr. Vieweg & Sohn, Braunschweig, Germany, 1963.

4. Lehnert, R., Rosenbaum, B., "Plasma Effects on Apollo Re-Entry Communications," Report X-513-64-8, Goddard Space Flight Center, Greenbelt, Maryland, January 1964.

5. Wittliff, C. E., Curtis, J. T., "Normal Shock Wave Parameters in Equilibrium Air," Cornell Aero. Lab., CAL Report No. CAL-111, November 1961.

6. Marrone, P. V., "Normal Shock Waves in Air: Equilibrium Composition and Flow Parameters for Velocities from 26,000 to 50,000 ft/sec," Cornell Aero. Lab., CAL Report No. AG-1729-A-2, August 1962.

7. Moeckel, W. E., Weston, K. C., "Composition and Thermodynamic Properties of Air in Chemical Equilibrium," NACA TN 4265, April 1958.

8. Hilsenrath, J., Klein, M., Woolley, H. W., "Tables of Thermodynamic Properties of Air Including Dissociation and Ionization from 1500° K to 15,000° K," AEDC TR-59-20, 1959.

9. Liepmann, H. W. Roshko, A., "Elements of Gasdynamics," Calcit Aeronautical Series, John Wiley & Sons, Inc., New York, Chapman & Hall, Ltd., London, 1957.

10. Woolley, H. W., "Effect of Dissociation on Thermodynamic Properties of Pure Diatomic Gases," NACA TN 3270, 1955.

11. "JANAF," Joint Army-Navy-Air Force Thermochemical Data, compiled and calculated by the Dow Chemical Company, Thermal Laboratory, Midland, Michigan, December 1960.

12. Evans, J. S., "Method for Calculation Effects of Dissociation on Flow Variables in the Relaxation Zone Behind Normal Shock Waves," NACA TN 3860, 1956.

13. Thoenes, J., "Inviscid High Temperature Hypersonic Flow of Air Past Pointed Bodies of Revolution," University of Alabama Research Institute, Huntsville, UARI Research Report No. 25, May 1965, supported by the U. S. Army Missile Command under Contract No. DA-01-009-AMC-166(Z).

14. Hansen, C. F., "Approximations for the Thermodynamic and Transport Properties of High-Temperature Air," NASA TR R-50, 1959.

15. Lee, J. F., Sears, F. W., Turcotte, D. L., "Statistical Thermodynamics," Addison-Wesley Publishing Company, Inc., 1963.

16. Herzfeld, K. F., et al., "Fundamental Physics of Gases," Princeton Aeronautical Paperbacks, Vol. 7, 1961.

17. Wray, K. L., "Chemical Kinetics of High Temperature Air," in "Hypersonic Flow Research," Progress in Astronautics and Rocketry, Vol. 7, Academic Press, 1962.

18. Bray, K. N. C., "Atomic Recombination in a Hypersonic Wind-Tunnel Nozzle," Journal of Fluid Mechanics, Vol. 6, Part 1, 1959.

19. Hall, J. G., Eschenroeder, A. G., and Marrone, P. V., "Inviscid Hypersonic Airflows with Coupled Non-Equilibrium Processes," Cornell Aeronautical Laboratory, Rep. No. AF-1413-A-2, 1962.

20. Dorodnitsyn, A. A., "A Contribution to the Solution of Mixed Problems of Transonic Aerodynamics," Advances in Aeronautical Sciences, Vol. 2, Pergamon Press, New York, 1959, pp. 832-844.

21. Belotserkovskii, O. M., "Flow Past a Circular Cylinder with a Detached Shock Wave," Doklady Akad. Nauk SSSR 113, No. 3, 1957. Also AVCO RAD-9-TM-59-66, 1959.

22. Holt, M., "Calculation of Pressure Distribution on Hypersonic Bodies by Belotserkovskii's Method," AVCO RAD-2-TM-58-45, 1958.

23. Traugott, S. C., "An Approximate Solution of the Supersonic Blunt Body Problem for Prescribed Arbitrary Axisymmetric Shapes," Martin Company, Res. Rep. No. 13, 1958.

24. Archer, R. D., "Inviscid Supersonic Flow Around an Elliptic Nose," Ph.D. Thesis, University of Minnesota, November 1963 (Adviser: R. Hermann).

25. Shih, W. C. L., Baron, J. R., Krupp, R. S., and Towle, W. J., "Non-Equilibrium Blunt Body Flow Using the Method of Integral Relations," Massachusetts Institute of Technology, Aerophysics Lab., Tech. Rep. 66. Also DDC AD No. 415 934, May 1963.

26. Yalamanchili, J., Hermann, R., "Non-Equilibrium Hypersonic Flow of Air in Hypersonic Nozzles and Around Blunt Bodies," University of Alabama Research Institute, Res. Rep. No. 3, May 1963. Also a short version with same title in Proceedings of Fifth International Symposium on Space Technology and Science, Tokyo, 1963.

27. Belotserkovskii, O. M., Golomazov, M. M., Shulishnina, N. D., "Calculation of Flow of Dissociated Air in Equilibrium Around Blunt Bodies with Detached Shock Wave," JCMMP, Vol. 4, No. 2, March-April 1964, pp. 306-316.

28. Hermann, R., Thoenes, J., "Hypersonic Flow of Air Past a Circular Cylinder with Non-Equilibrium Oxygen Dissociation Including Dissociation of the Free Stream," Paper presented at the VI European Aeronautical Congress at Munich, Germany, September 1965. To be published in the Yearbook 1965, Wissenschaftliche Gesellschaft fuer Luft-und Raumfahrt, Friedr. Vieweg & Sohn, Braunschweig, Germany, 1965. Also University of Alabama Research Institute, Huntsville, UARI Research Report No. 28, September 1965.

29. Yalamanchili, J., Thoenes, J., "Normal and Oblique Shock Wave Parameters for Various Dissociated Upstream Conditions in Air with Frozen Composition Across the Shock," University of Alabama Research Institute, Res. Rep. No. 4, 1964.

30. Conti, R. J., "Stagnation Equilibrium Layer in Non-Equilibrium Blunt-Body Flows," AIAA Journal, Vol. 2, November 1964, pp. 2044-2046.

31. Melnik, W. L., "Supersonic and Hypersonic Flow of an Ideal Gas About Elliptic Cones by the Method of Integral Relations," Ph.D. Thesis, University of Minnesota, February 1964 (Adviser: R. Hermann).

32. Feldman, S., "Hypersonic Conical Shocks for Dissociated Air in Thermodynamic Equilibrium," Jet Propulsion, Vol. 27, No. 12, Dec. 1957.

33. Romig, M. F., "Application of Hypersonic Similarity Rule to Conical Flow of Dissociated Air," Aero Space Engineering, March 1959.

34. Romig, M. F., "Conical Flow Parameters for Air in Dissociation Equilibrium," Convair Sci. Res. Report No. 7, 1960.

35. Sedney, R., Gerber, N., "Non-Equilibrium Flow Over a Cone," IAS Paper No. 63-71, also AIAA J., Vol. 1, No. 11, November 1963.

36. Capiaux, R., Washington, M., "Non-Equilibrium Flow Past a Wedge," AIAA J., Vol. 1, No. 3, March 1963, pp. 650-660.

37. South, J. C., "Application of Dorodnitsyn's Integral Method to Non-Equilibrium Flows Over Pointed Bodies," NASA TN D-1942, August 1963.

38. Newman, P. A., "Approximate Calculation of Hypersonic Conical Flow Parameters for Air in Thermodynamic Equilibrium," NASA TN D-2058, January 1964.

39. "U.S. Standard Atmosphere," 1962, U.S. Government Printing Office, Washington 25, D. C.

40. Daniels, S., and Alberty, R. A., "Physical Chemistry," John Wiley & Sons, Inc. New York, 1961. Page 326.

TABLE I AIR MODEL AND PHYSICAL CONSTANTS

Simplified Air Model			
1	O_2	21.00	Vol %
2	N_2	79.00	Vol %
3	M	28.8503	kg/kmol
4	$Z_o = p_o/R\,\rho_o\,T_o$	1	
5	ρ_o	1.2872	kg/m^3
Standard Conditions			
6	T_o	273.15	°K
7	p_o	$1.01325 \cdot 10^5$	N/m^2
Universal Constants			
8	R^*	8314.32	J/kmol °K
9	N_A	$6.02257 \cdot 10^{26}$	$kmol^{-1}$
10	h	$6.6237 \cdot 10^{-34}$	J · sec

Defined are Nos. 1, 2, 4. Calculated are Nos. 3 and 5. Nos. 6, 7 8, 9 are taken from Reference 39. No. 10 taken from Reference 15.

TABLE II ATOMIC AND MOLECULAR CONSTANTS

Particle	Molecular Weight M	Rotational Temperature $\varkappa\theta_r$	Vibrational Temperature θ	Char. Temp. of Dissoc. D'	Electronic Degeneracy g_i	Electronic Energy ϵ_i/k
	kg/kmol	°K	°K	°K		°K
N_2	28.0134	5.78	3390	113200	1	0
O_2	31.9988	4.16	2270	59366	3	0
					2	11390
O	15.9994				5	0
					3	228
					1	326

The values for M are taken from Reference 39. All other values are taken from References 14, 15, 16.

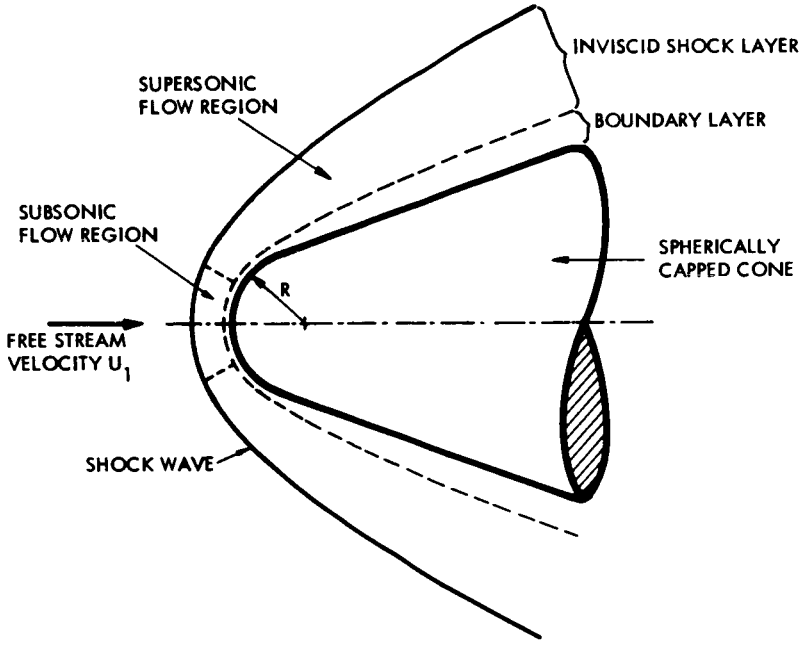

FIG. 1. BLUNT BODY CONFIGURATION AND FLOW FIELD (SCHEMATIC).

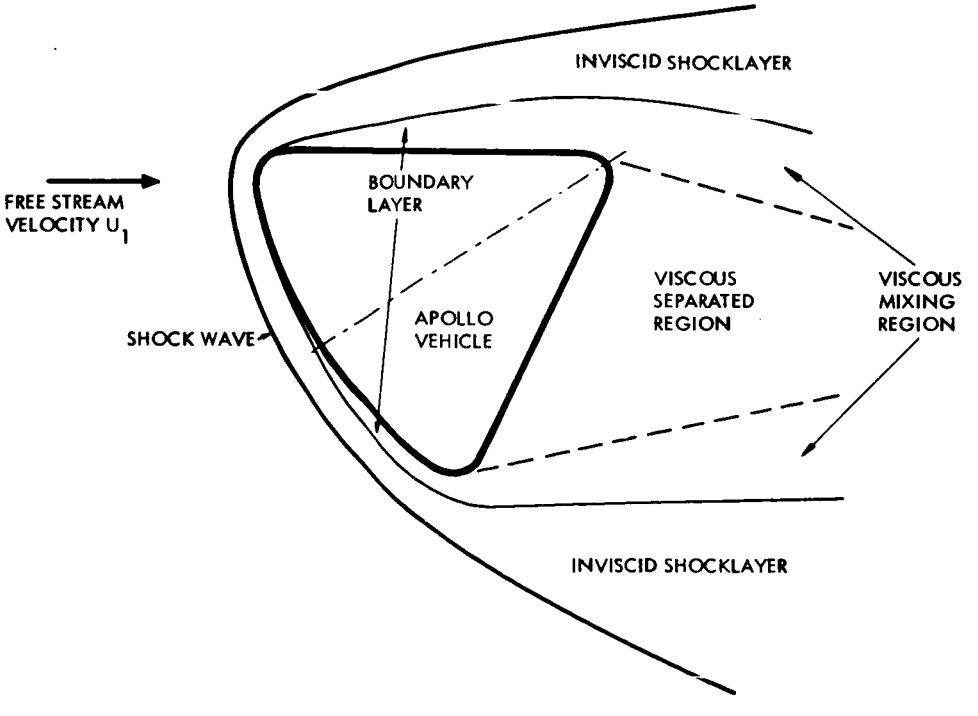

FIG. 2. HYPERSONIC FLOW REGIONS (SCHEMATIC) FOR APOLLO VEHICLE, REF.4.

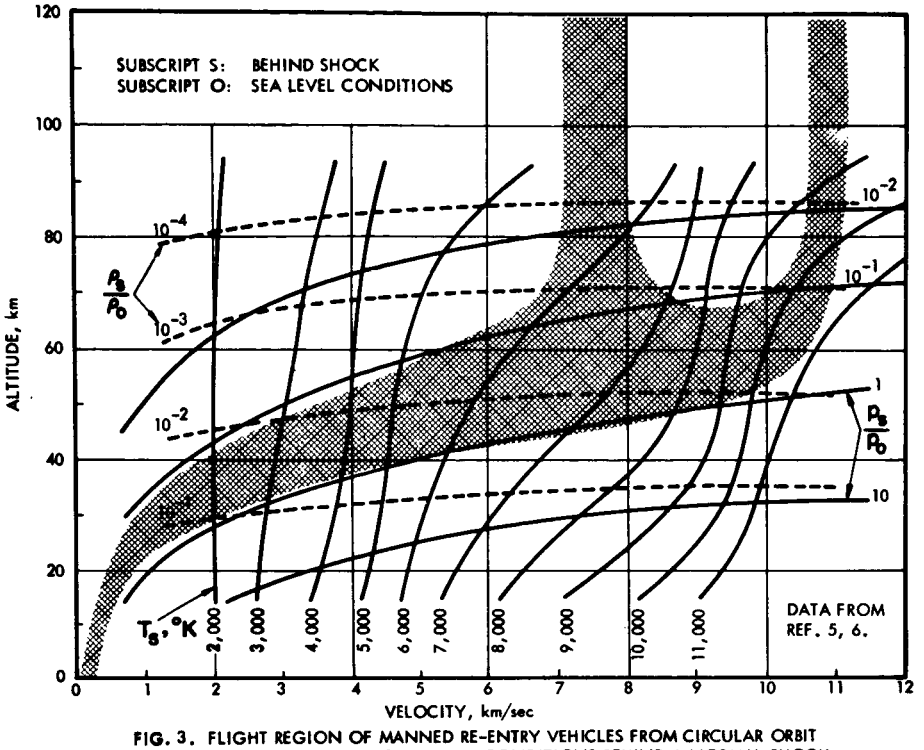

FIG. 3. FLIGHT REGION OF MANNED RE-ENTRY VEHICLES FROM CIRCULAR ORBIT AND LUNAR RETURN. ALSO EQUILIBRIUM CONDITIONS BEHIND A NORMAL SHOCK.

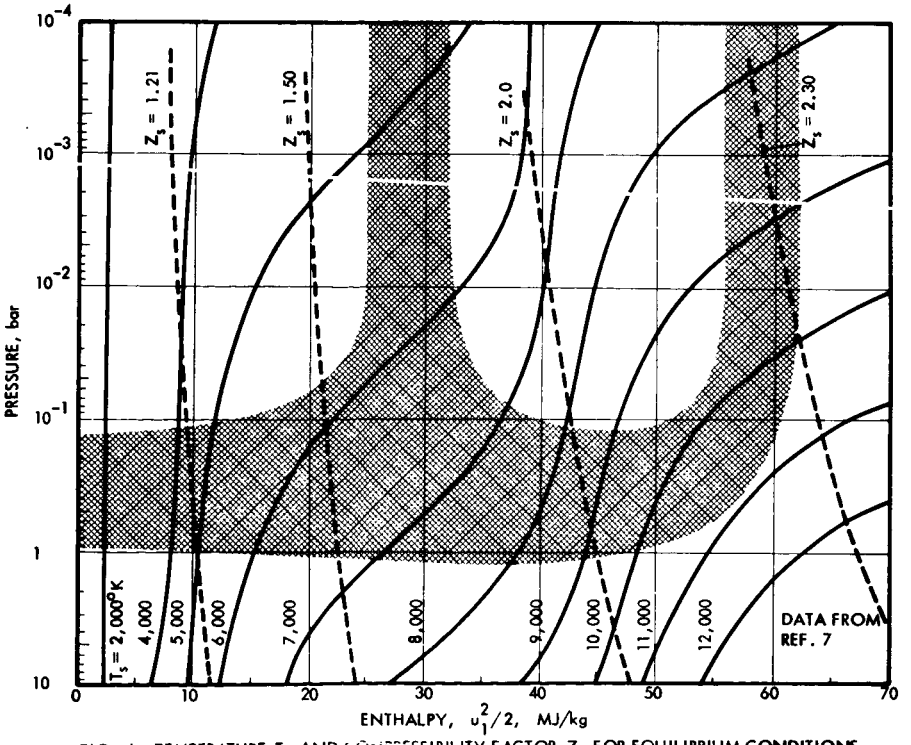

FIG. 4. TEMPERATURE T_s AND COMPRESSIBILITY FACTOR Z_s FOR EQUILIBRIUM CONDITIONS BEHIND A NORMAL SHOCK. ALSO FLIGHT REGION OF MANNED RE-ENTRY VEHICLES FROM CIRCULAR ORBIT AND LUNAR RETURN.

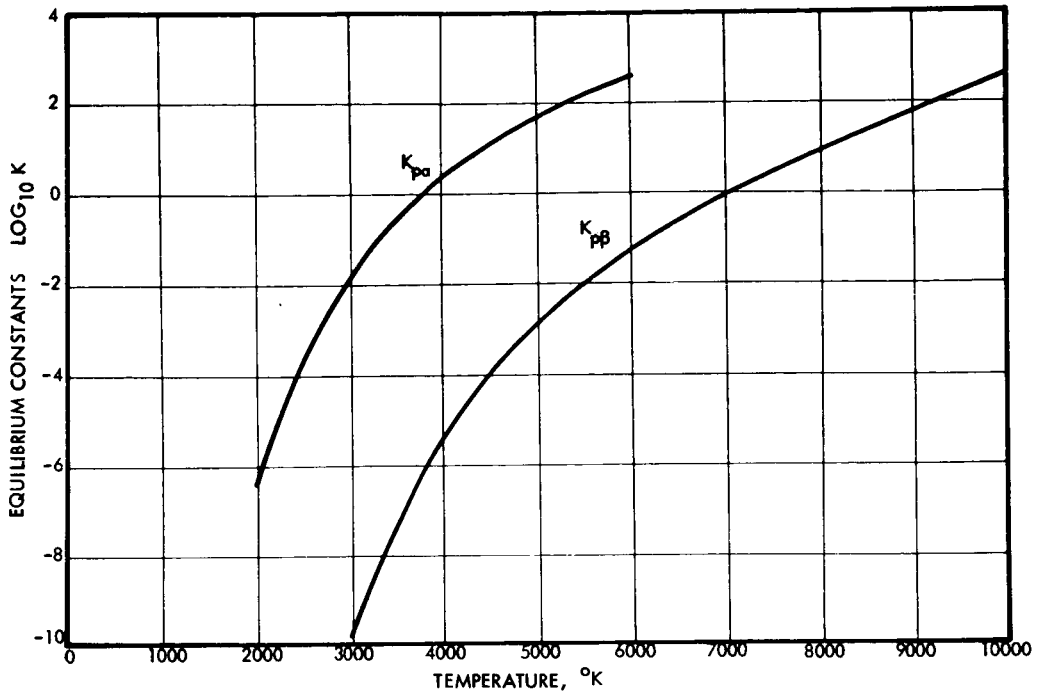

FIG. 5. OXYGEN AND NITROGEN EQUILIBRIUM CONSTANTS $K_{p\alpha}$ AND $K_{p\beta}$ AS FUNCTION OF TEMPERATURE

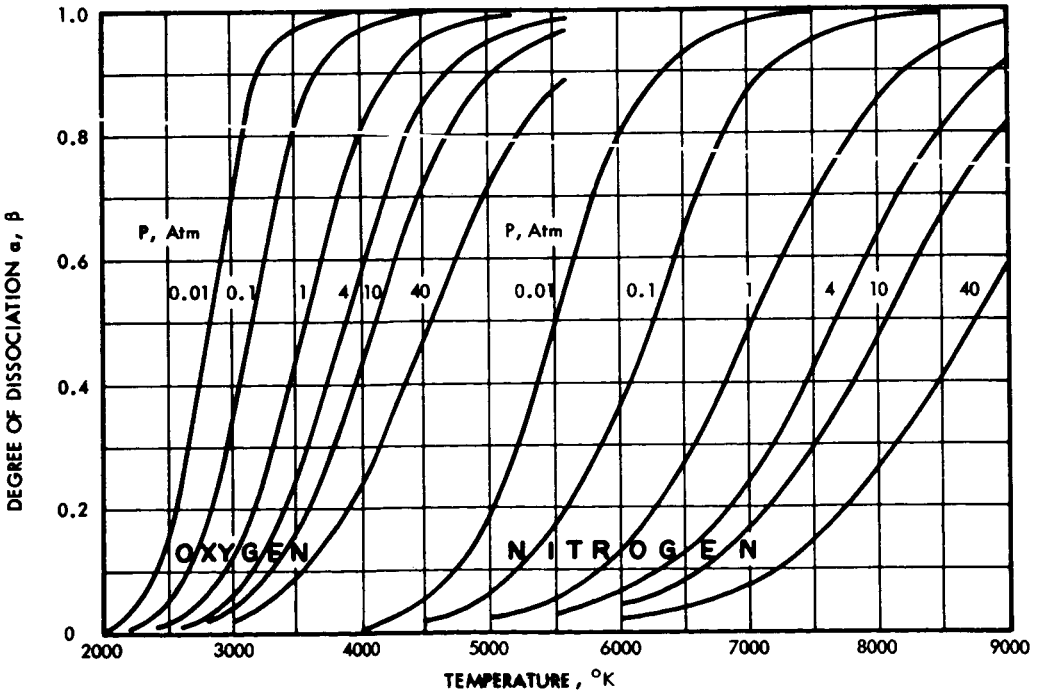

FIG. 6. DEGREE OF OXYGEN DISSOCIATION α AND NITROGEN DISSOCIATION β AS FUNCTION OF TEMPERATURE AND PRESSURE, CALCULATED FOR SIMPLIFIED AIR-MODEL IN EQUILIBRIUM.

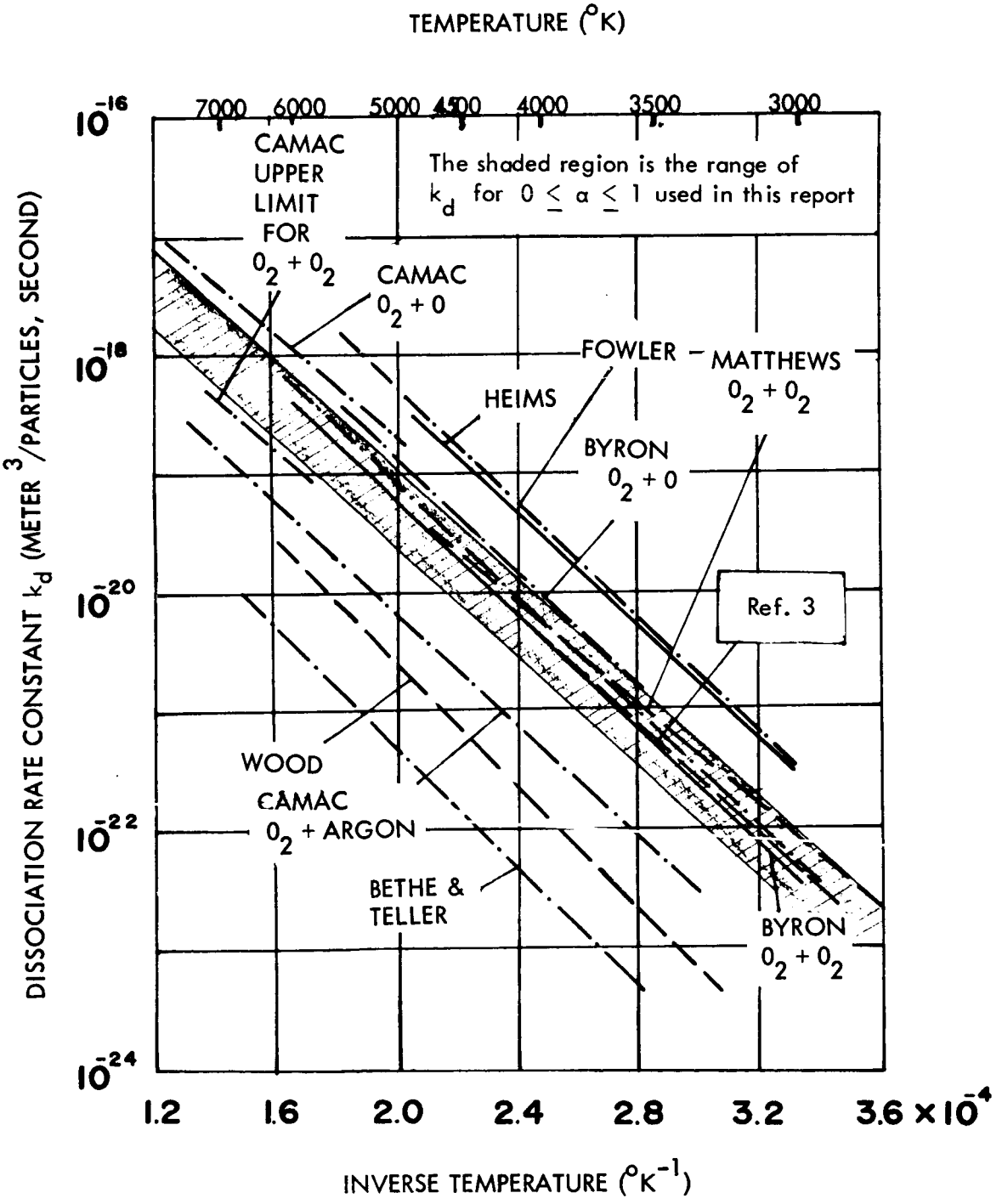

FIG. 7. OXYGEN DISSOCIATION RATE CONSTANT FOR VARIOUS COLLIDING BODIES, OTHER AUTHORS AND THIS REPORT

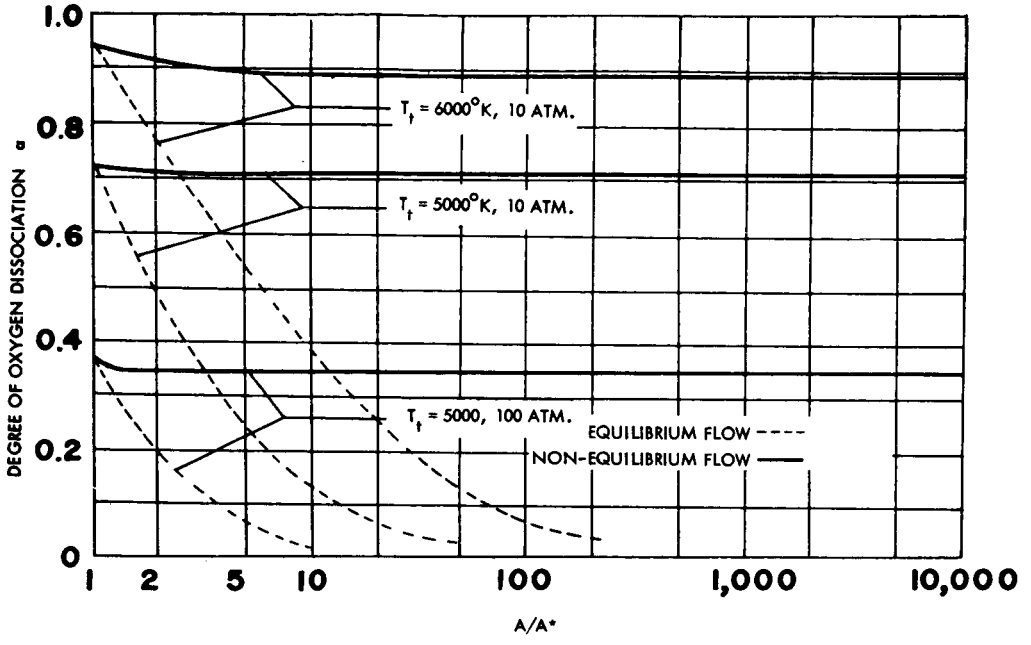

FIG. 8. DEGREE OF OXYGEN DISSOCIATION ALONG HYPERSONIC NOZZLE IN EQUILIBRIUM AND NON-EQUILIBRIUM FLOW

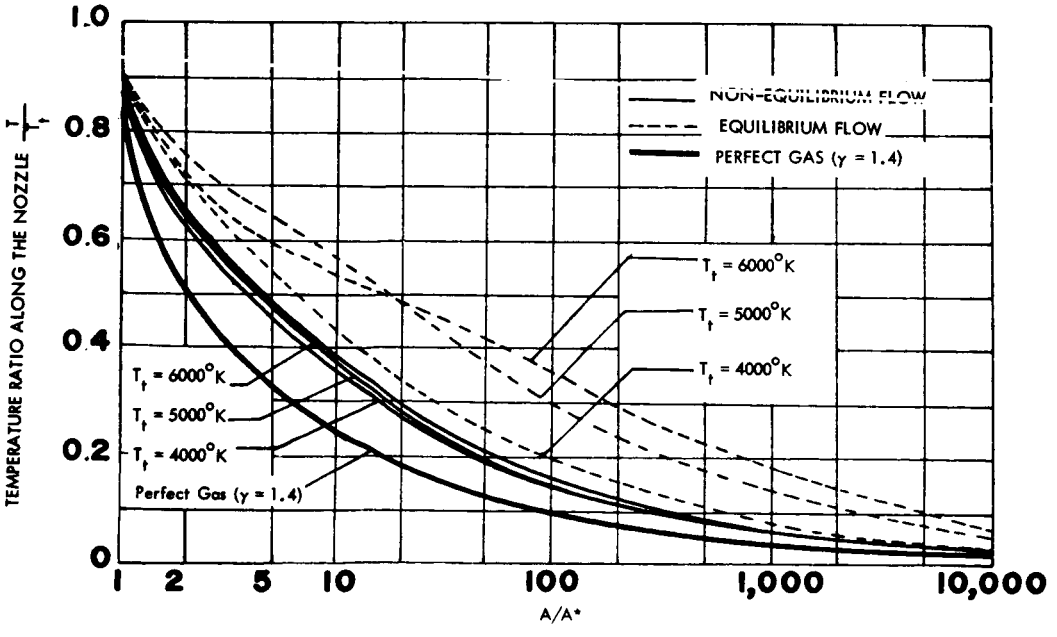

FIG. 9. TEMPERATURE DISTRIBUTION ALONG THE HYPERSONIC NOZZLE IN EQUILIBRIUM AND NON-EQUILIBRIUM FLOW FOR P_t = 50 atm.

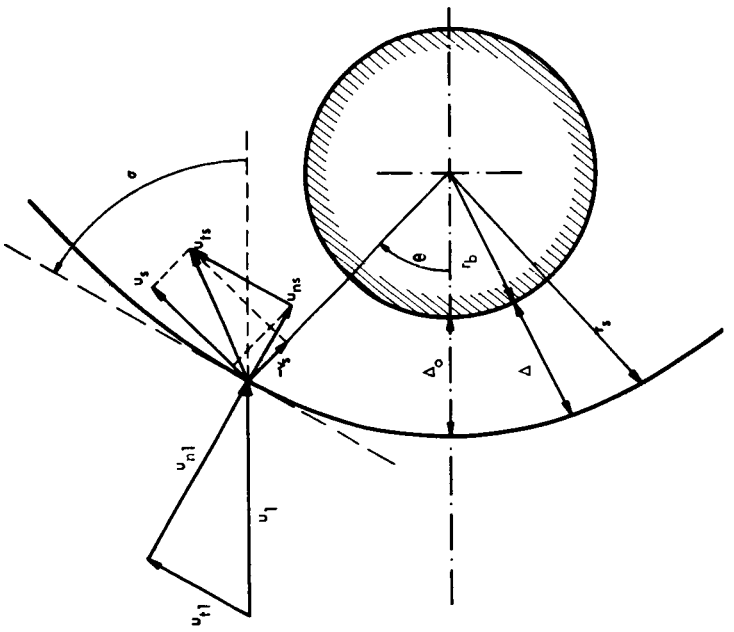

FIG. 11. COORDINATE SYSTEM AND SHOCK WAVE GEOMETRY ON CIRCULAR CYLINDER

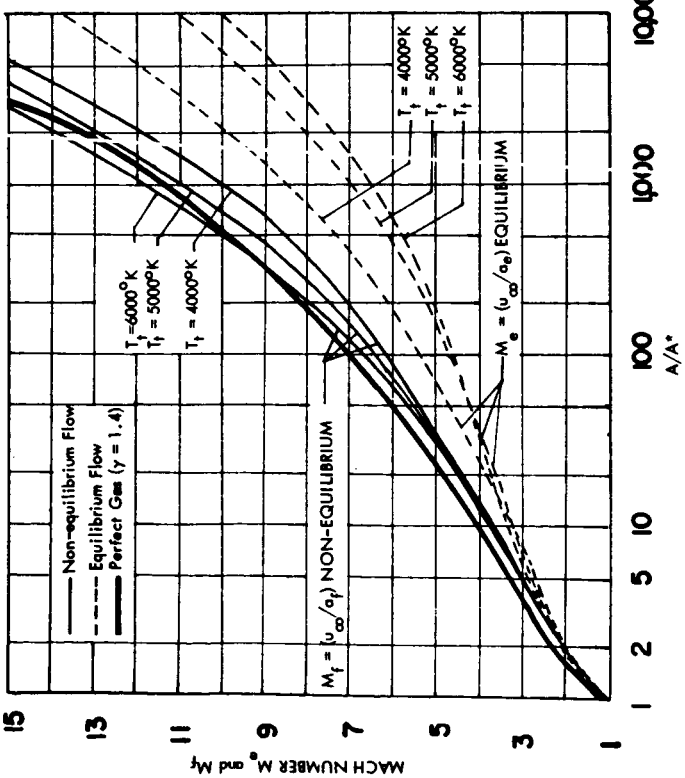

FIG. 10. MACH NUMBER DISTRIBUTION ALONG HYPERSONIC NOZZLE IN EQUILIBRIUM AND NON-EQUILIBRIUM FLOW

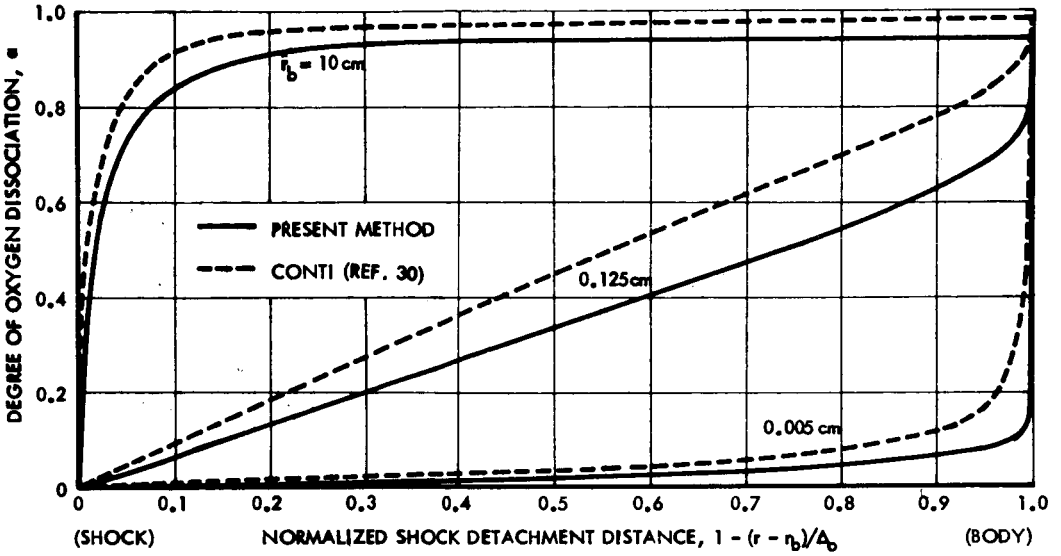

FIG. 12. DEGREE OF OXYGEN DISSOCIATION ALONG STAGNATION STREAMLINE FOR VARIOUS BODY RADII (Flight Speed 4300 m/sec, Altitude 30 km)

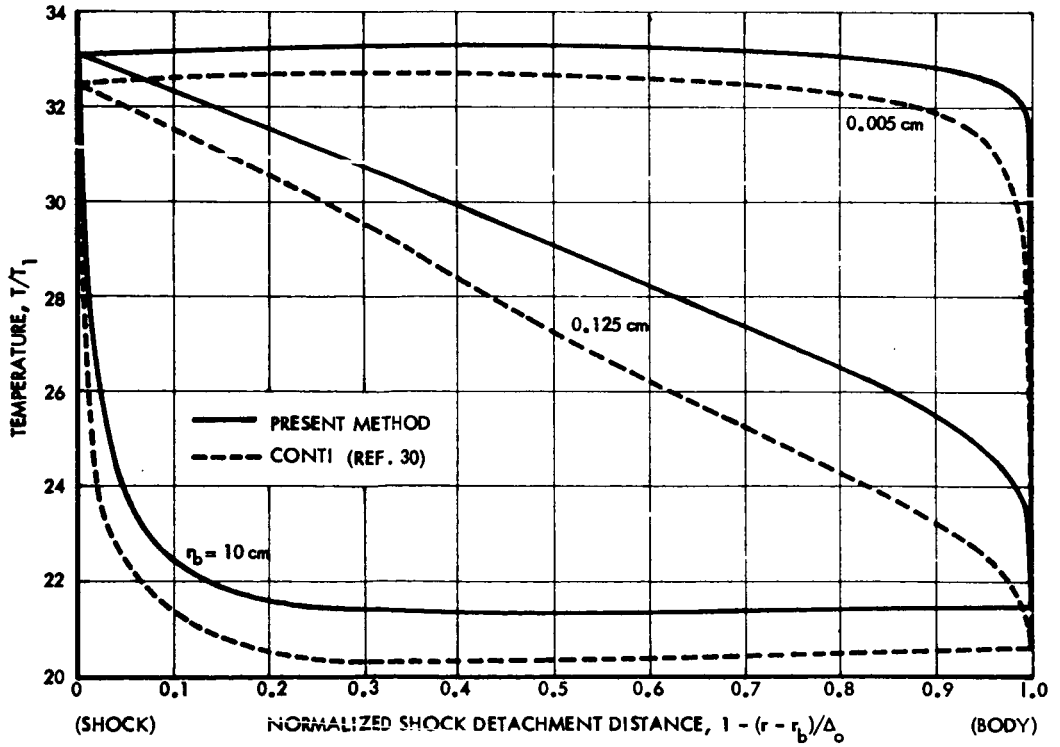

FIG. 13. TEMPERATURE ALONG STAGNATION STREAMLINE FOR VARIOUS BODY RADII (Flight Speed 4300 m/sec, Altitude 30 km)

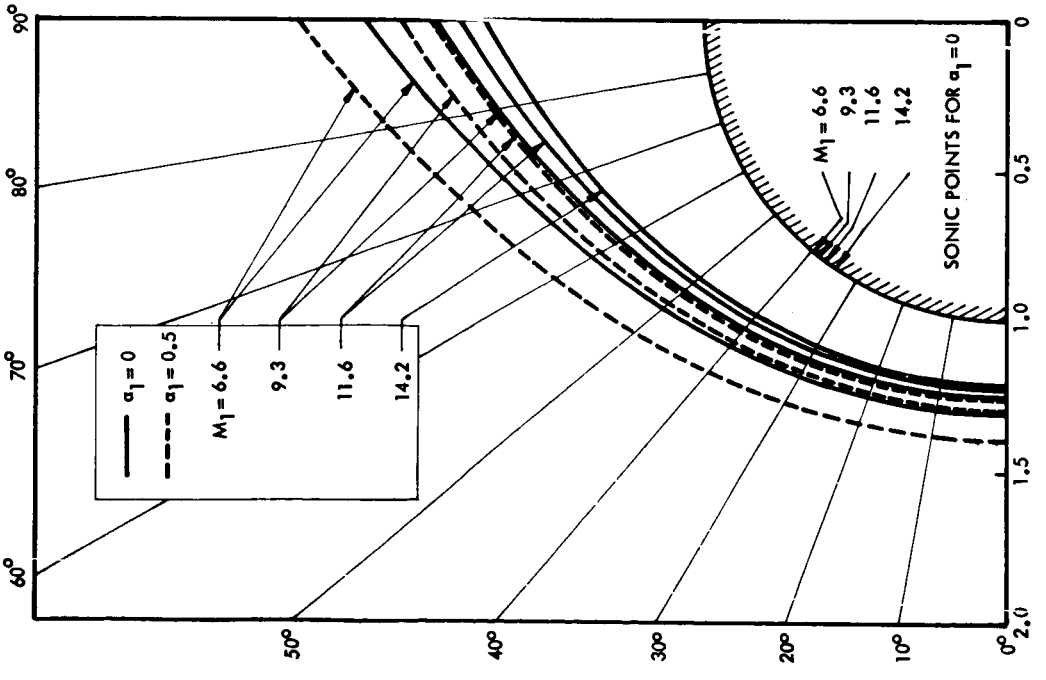

FIG. 14. CALCULATED SHOCK SHAPES FOR CIRCULAR CYLINDER (r_b = 10 cm, Altitude 30 km)

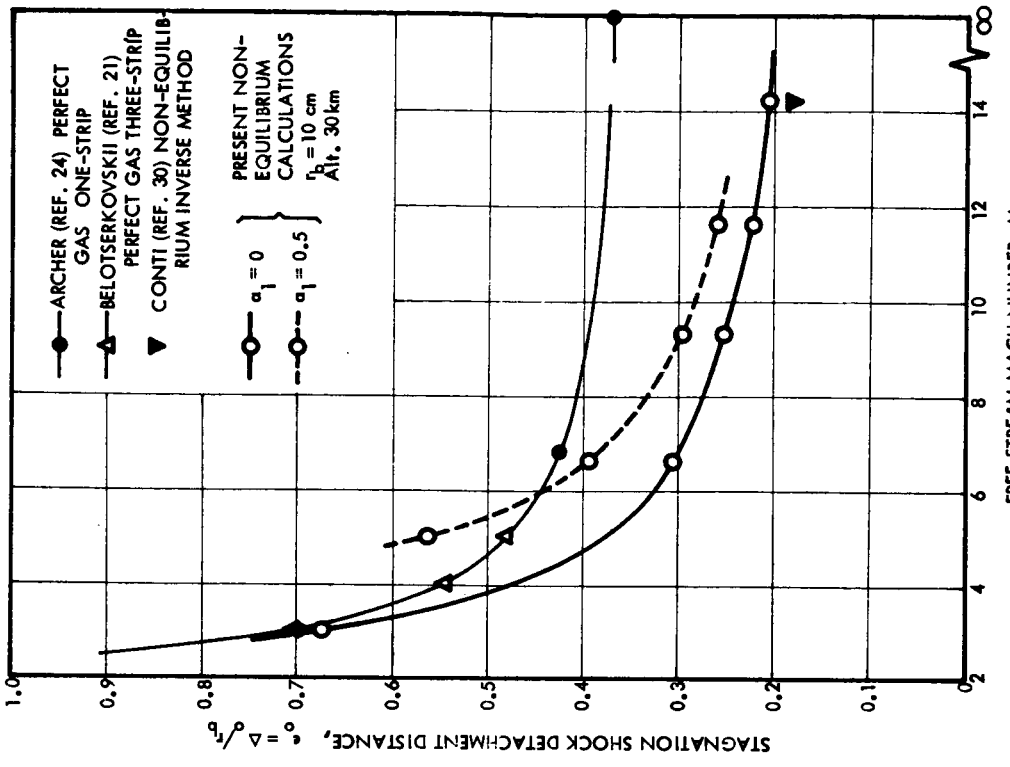

FIG. 15. STAGNATION SHOCK DETACHMENT DISTANCE ON CIRCULAR CYLINDER

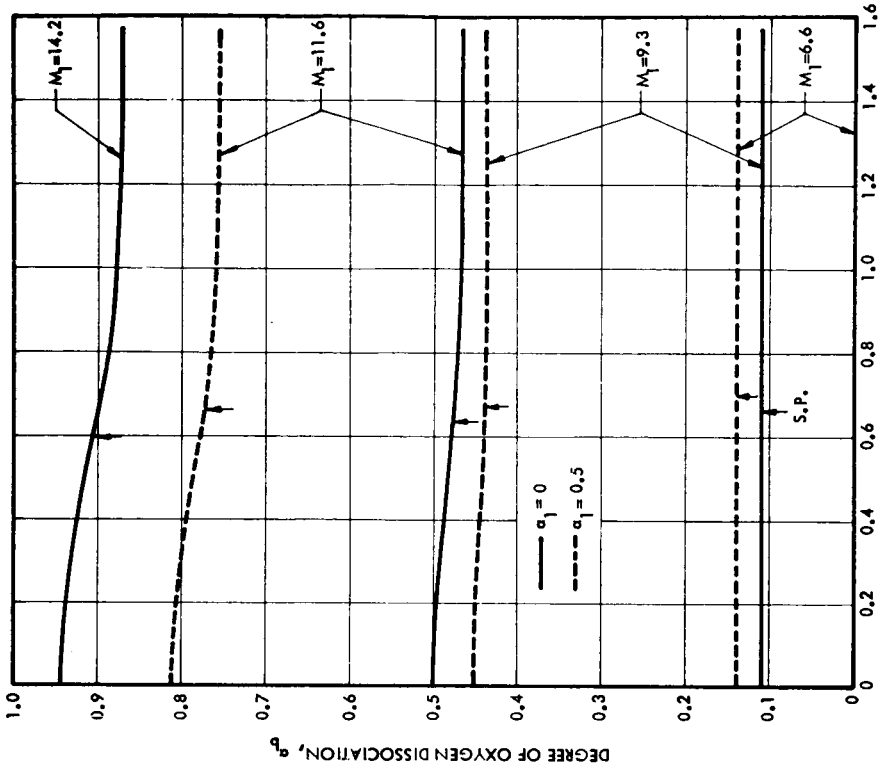

FIG. 17. DEGREE OF OXYGEN DISSOCIATION ALONG BODY SURFACE (r_b = 10 cm, Altitude 30 km)

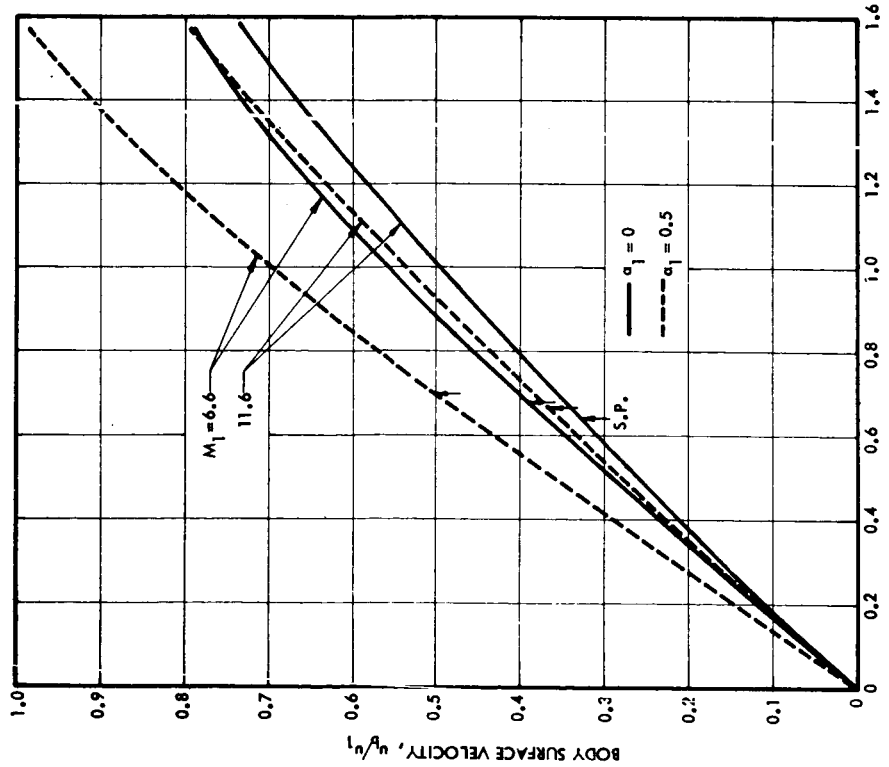

FIG. 16. VELOCITY DISTRIBUTION ALONG BODY SURFACE (r_b = 10 cm, Altitude 30 km)

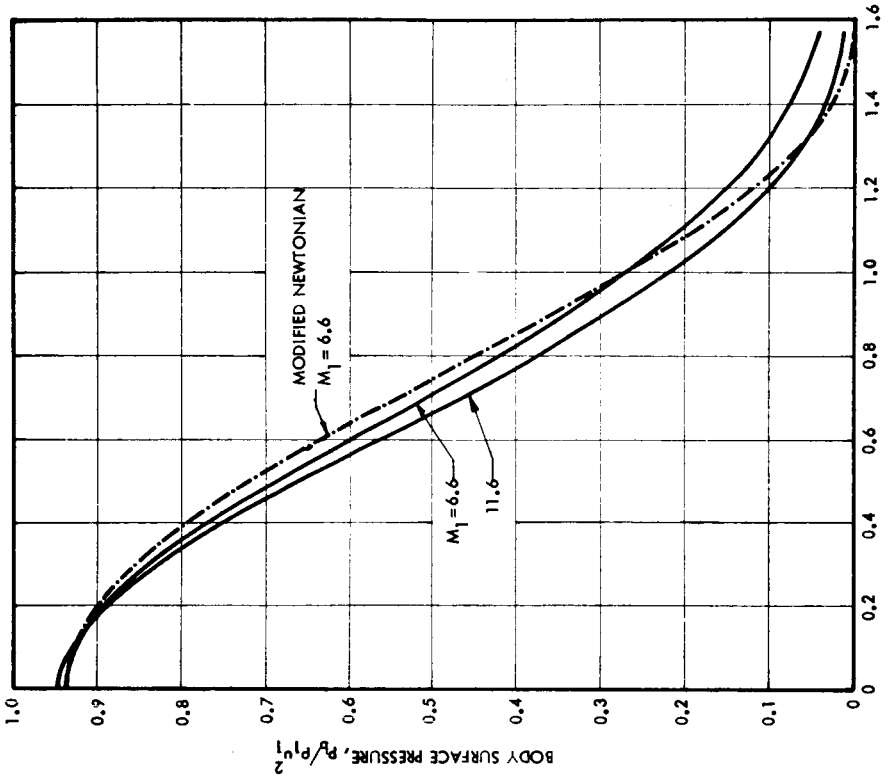

FIG. 19. PRESSURE DISTRIBUTION ALONG BODY SURFACE (r_b = 10 cm, Altitude 30 km)

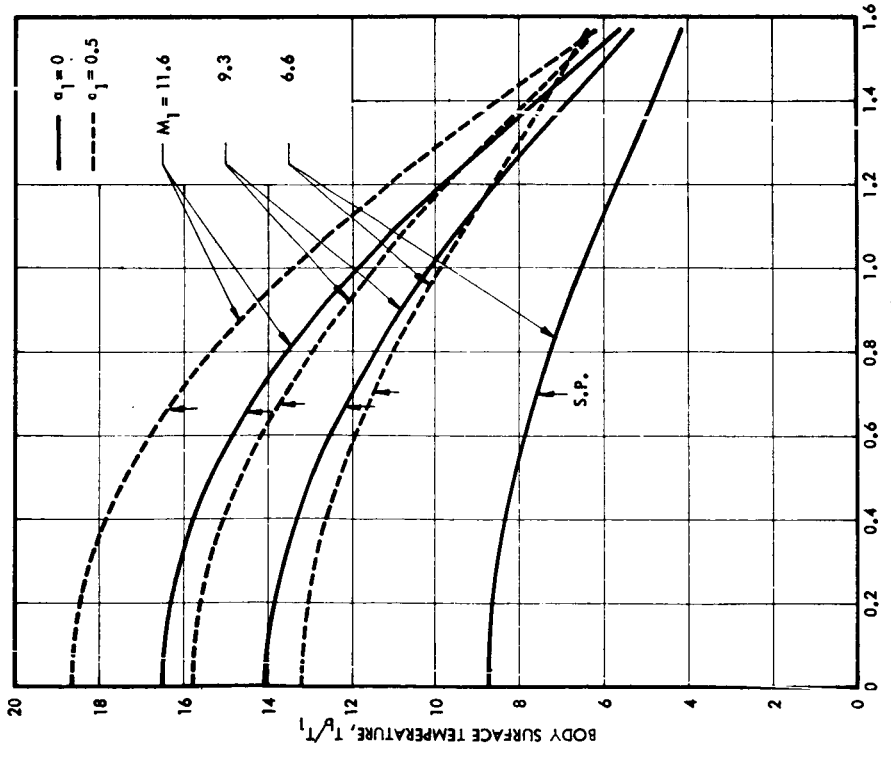

FIG. 18. TEMPERATURE DISTRIBUTION ALONG BODY SURFACE (r_b = 10 cm, Altitude 30 km)

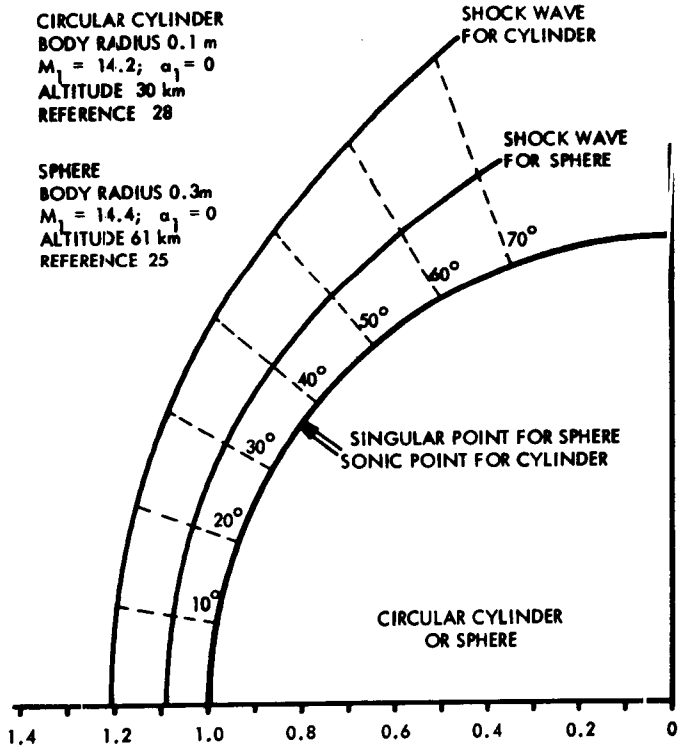

FIG. 20. SHOCK WAVES IN FRONT OF A CYLINDER AND A SPHERE FOR NON-EQUILIBRIUM FLOW.

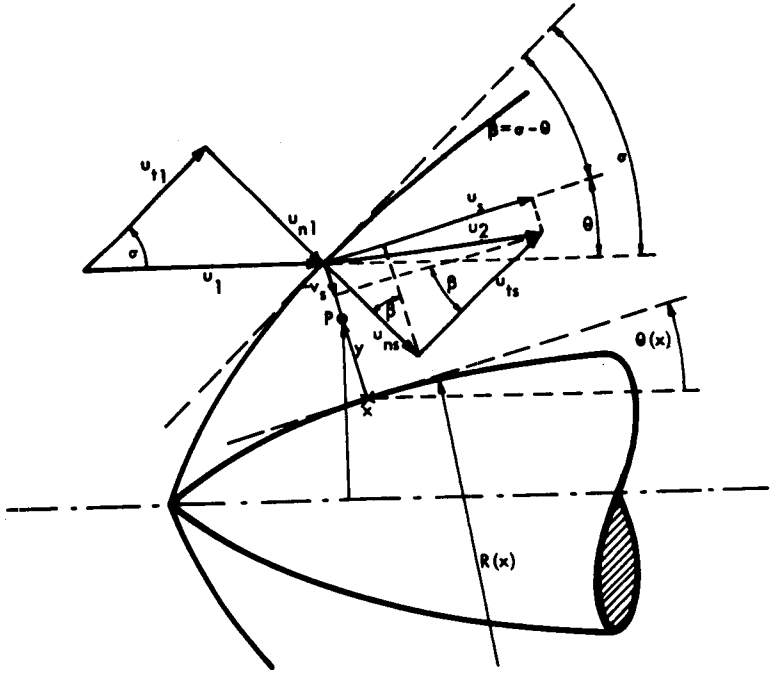

FIG. 21. COORDINATE SYSTEM AND SHOCK GEOMETRY ON ARBITRARY CIRCULAR POINTED BODY.

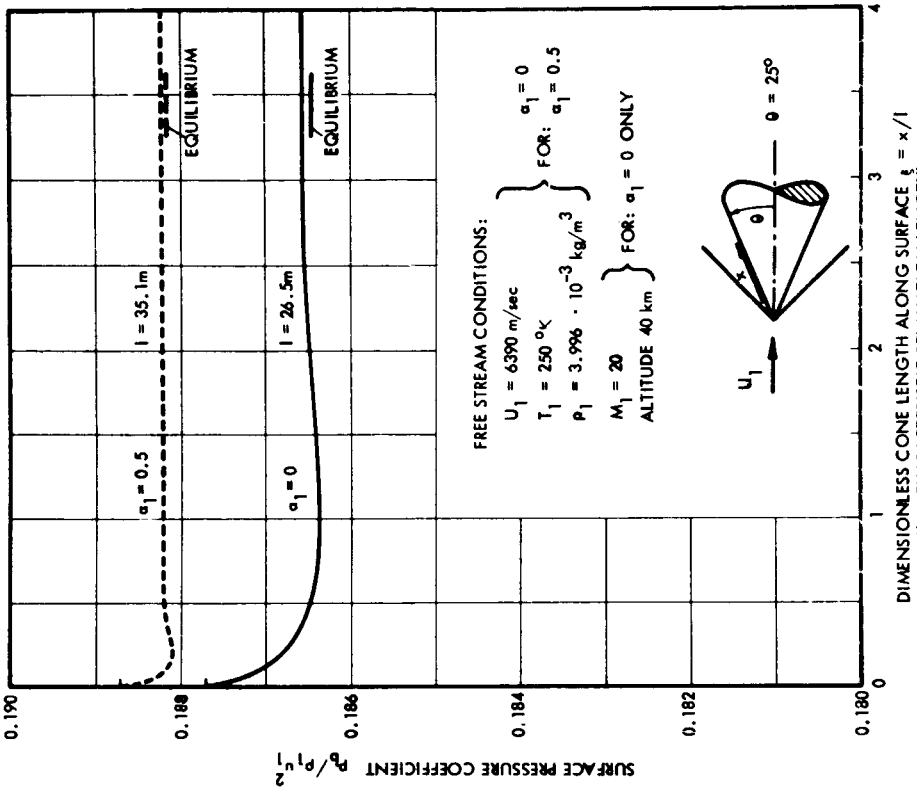

FIG. 23. PRESSURE p_b ON BODY SURFACE AS FUNCTION OF CONE LENGTH x/l FOR CHEMICAL NON-EQUILIBRIUM FLOW AROUND A CIRCULAR CONE.

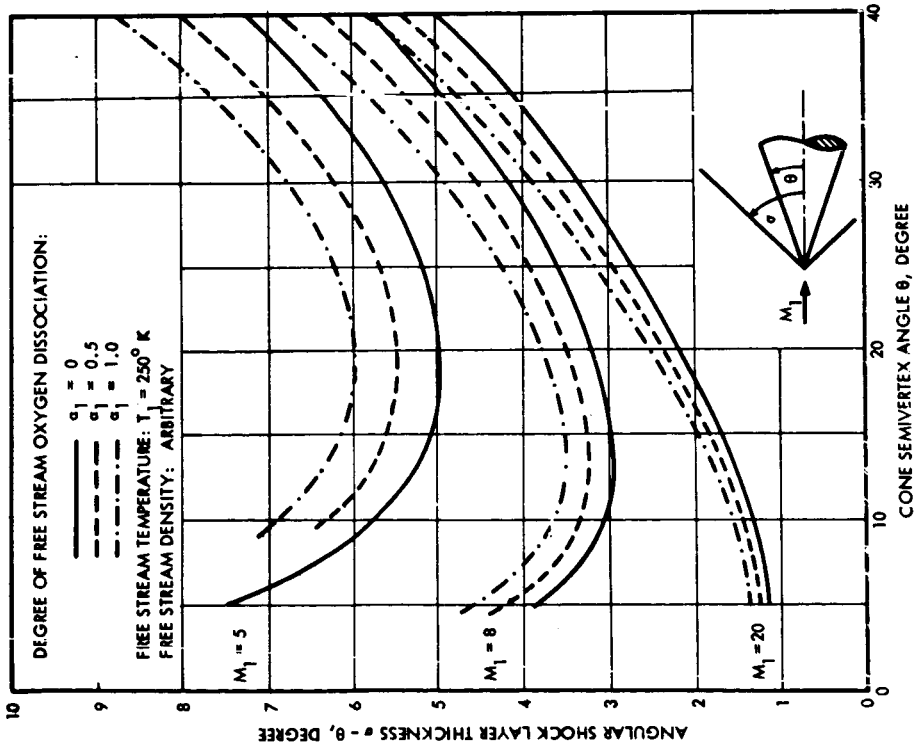

FIG. 22. SHOCK LAYER THICKNESS AS FUNCTION OF CONE SEMIVERTEX ANGLE FOR CHEMICALLY AND VIBRATIONALLY FROZEN FLOW AROUND A CIRCULAR CONE. INCLUDED IS FREE STREAM OXYGEN DISSOCIATION AT 3 MACH NUMBERS.

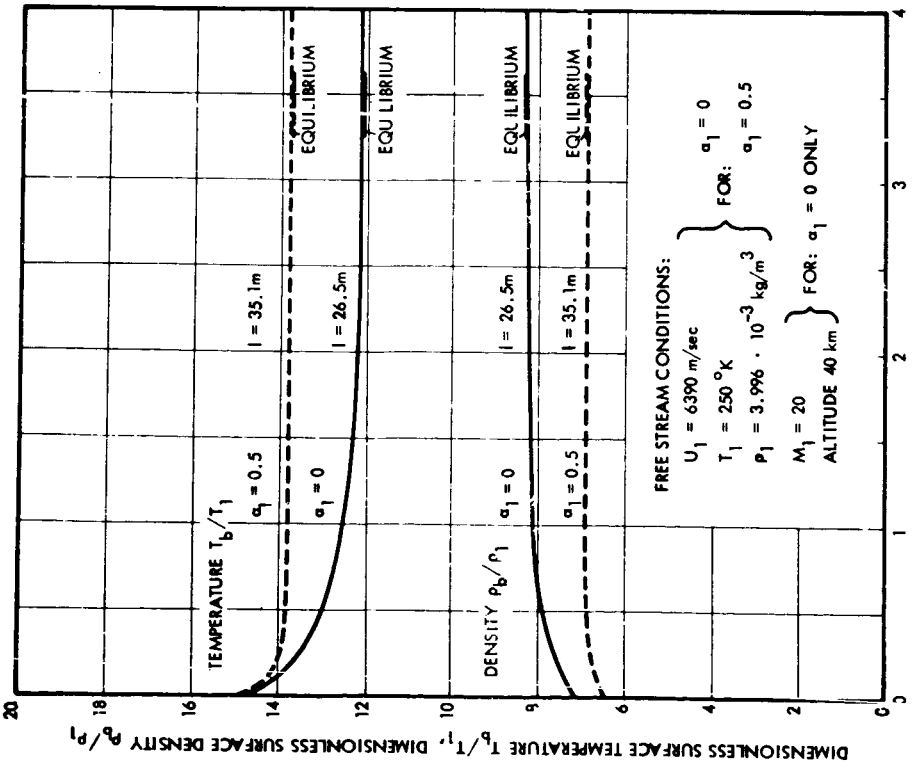

FIG. 24. TEMPERATURE T_b AND DENSITY ρ_b ON BODY SURFACE AS FUNCTION OF CONE LENGTH x/l FOR CHEMICAL NON-EQUILIBRIUM FLOW AROUND A CIRCULAR CONE (SEMIVERTEX ANGLE $\theta = 25°$).

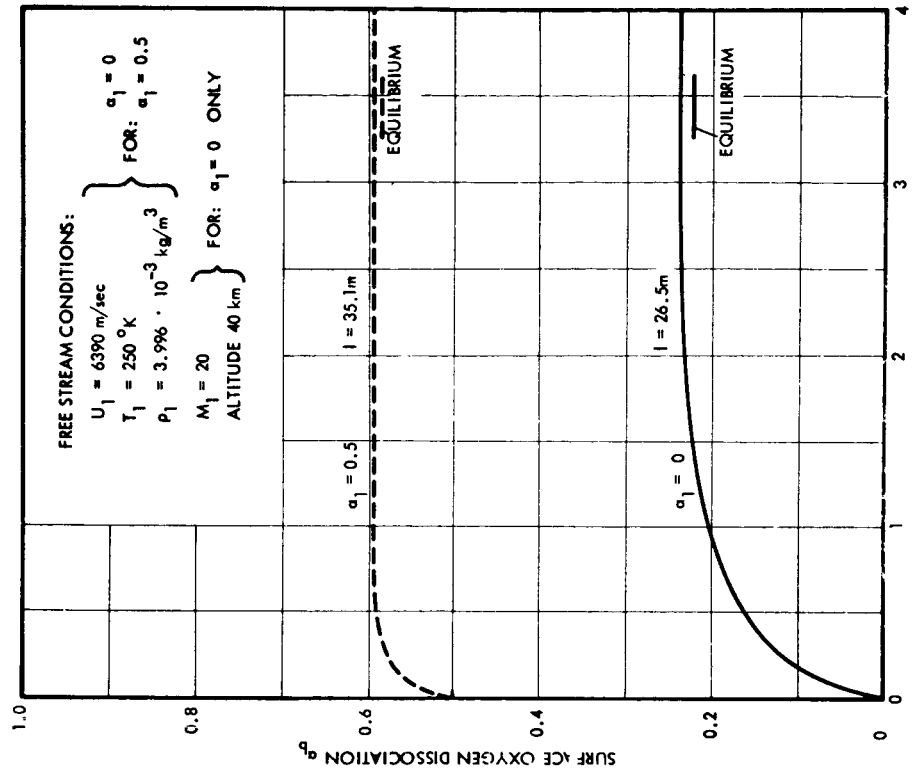

FIG. 25. OXYGEN DISSOCIATION α_b ON BODY SURFACE AS FUNCTION OF CONE LENGTH x/l FOR CHEMICAL NON-EQUILIBRIUM FLOW AROUND A CIRCULAR CONE (SEMIVERTEX ANGLE $\theta = 25°$).

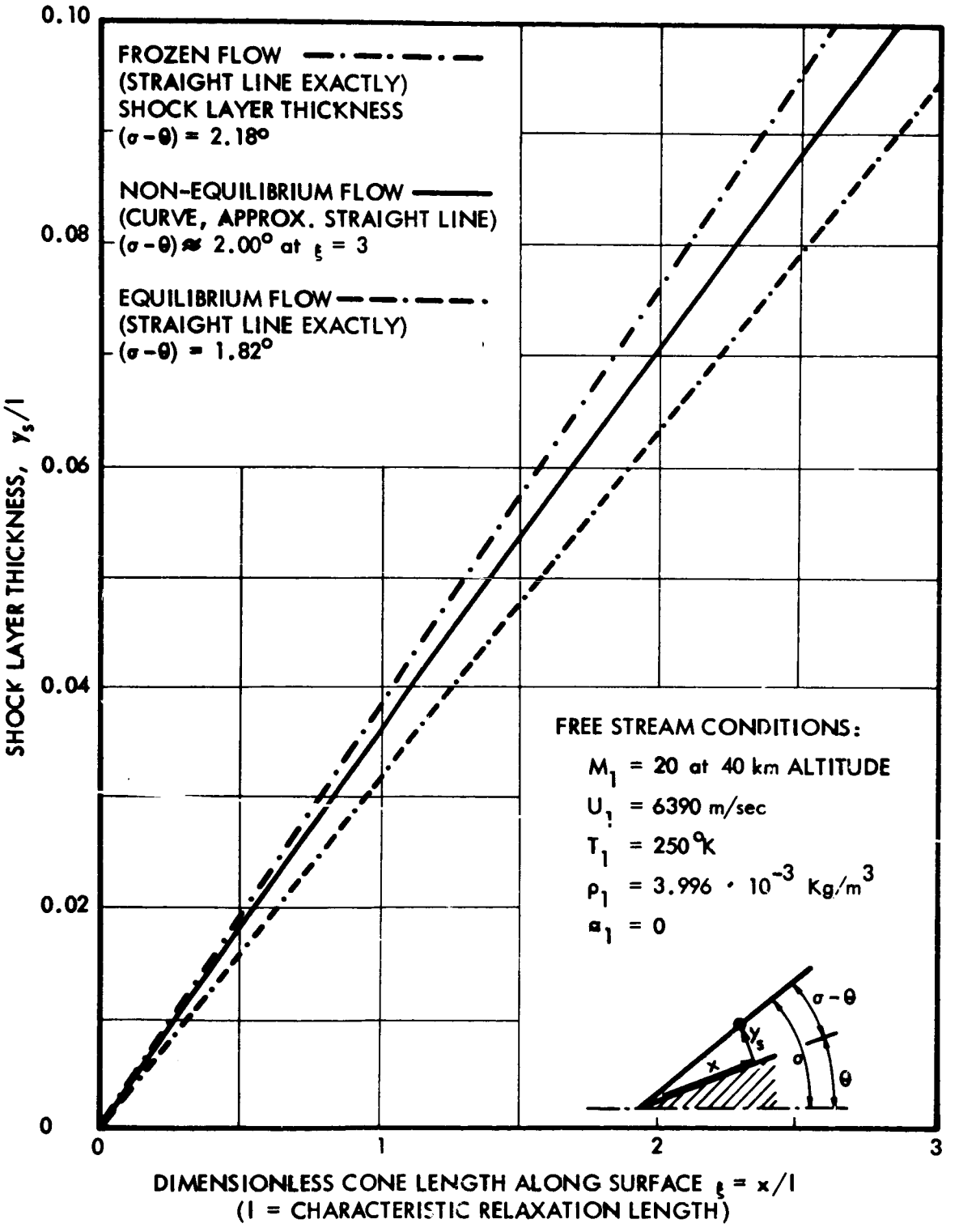

FIG. 26. SHOCK LAYER THICKNESS y_s/l AS FUNCTION OF CONE LENGTH x/l FOR FROZEN, NON-EQUILIBRIUM, AND EQUILIBRIUM FLOW AROUND A CIRCULAR CONE (SEMIVERTEX ANGLE $\theta = 25^\circ$; $l = 26.5$m).